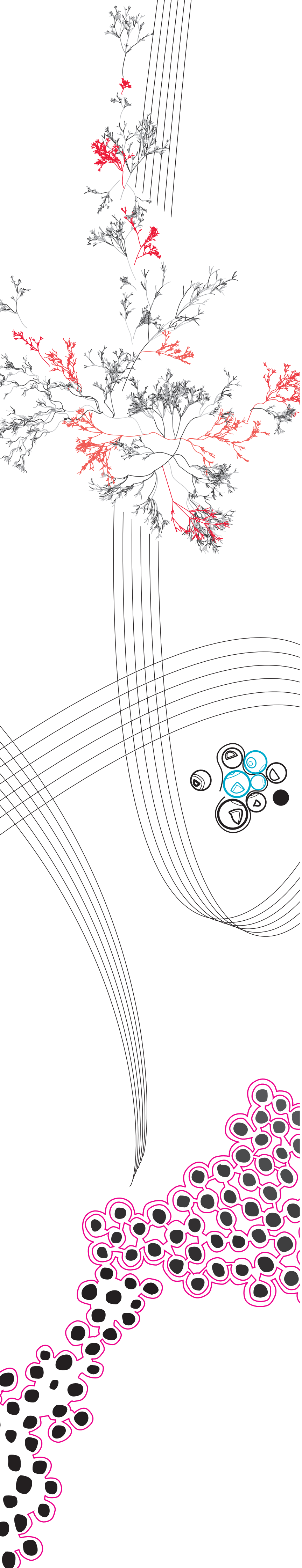

5th June 2015

BACHELOR ASSIGNMENT

Ultrasonic control over nanorod orientation in evaporative assembly

Tim Boulogne
Floor Derkink

Faculty of Science and Technology (S&T)
Physics of Interfaces and Nanomaterials (PIN)

Exam committee:
I. Ahmad M.Sc.
Dr. E.S. Kooij
Dr. J.W.J. Verschuur

UNIVERSITY OF TWENTE.

Summary

In this thesis the effect of ultrasonic agitation on the orientation and self-assembly of gold nanoparticles was investigated on both SiO_2 and HOPG substrates using scanning electron microscopy (SEM) and atomic force microscopy (AFM). For SiO_2 substrates, the effect was analyzed using two different solutions; one (solution R) containing gold nanorods (GNRs) while the other (solution RS) contained both GNRs and gold nanospheres all with approximately equal dimensions. For HOPG substrates, only the solution containing GNRs was used. After synthesis of the solutions containing gold nanoparticles using the seed-mediated method, the solutions were investigated using UV-VIS spectroscopy in order to characterize them and verify the aspect ratio (AR) of the GNRs. Furthermore, the absorption spectra were simulated to determine the ARs of the GNRs more correctly by taking into account that the ARs follow a normal distribution. Droplets were deposited on both types of substrates, of which some where left to dry undisturbed while others were placed in an ultrasonic bath. Evaporation of the solvent let to coffee-stain rings which were then further investigated using SEM and AFM. SEM images were used to measure the lengths and widths of GNRs to determine their ARs, to measure the lengths of chains of side-by-side assembled GNRs and to measure the angles of GNRs with respect to the step edges of HOPG. AFM images were used to determine the position of GNRs when aligned to step edges.

For SiO_2 substrates, results suggest that ultrasonic agitation did not have a significant effect on solution R during evaporation even though some of the assembled chains of GNRs were longer, but this is probably attributed to an unintentional rise in temperature of the ultrasonic bath during evaporation. For solution RS, ultrasonic agitation did seem to have a tremendous effect. Instead of a neat phase separation with side-by-side assembled GNRs interspersed by regions of gold nanospheres which was seen in the undisturbed case, the gold nanospheres seem to have disappeared from the edge of the ring and GNR chains seem to be shorter. Results on HOPG also suggest that ultrasonic agitation has an effect, since GNRs are less often aligned parallel to step edges and seem to be near step edges less often in general. Further research should be done in order to rule out that the observations that were made were not caused by a rise in temperature during evaporation or other factors that had an influence that were not kept constant.

Contents

1 Introduction

In recent years, gold nanoparticles have gained much attention in research due to their unique properties that deviate from those of bulk materials [1–7]. Gold nanoparticles have a wide range of potential applications including chemical sensing, biological imaging [8–10] and drug delivery [11]. The size and shape of these nanoparticles seem to affect their optical properties [1–3, 9, 12–16]. For example, a gold nanosphere with a diameter of about 10 nm will make a solution turn red, while a gold nanorod (GNR) with an aspect ratio (AR = length/width) of 3 will make a solution turn blue. Since bulk gold material has a yellow color, these are divergent properties that can be explained by how light interacts with the material [17]. This effect is now understood to be due to surface plasmons, which have been defined as 'collective oscillations of conduction band electrons in a metal, when the metal particle size approaches the electron mean free path length ($\sim$10-100 nm)' [8].

In order to use gold nanoparticles in applications, it is important to know how to synthesize nanoparticles of certain shapes and sizes. The most common and efficient method to synthesize gold nanoparticles is the seed-mediated method [8, 17–19]. This method combines a seed solution containing gold nanoparticles with a growth solution of which the parameters can be tuned in order to control the shape of the gold nanoparticles during the growth process [20].

Another factor that should be taken into consideration for applications is the interactions between these nanoparticles and their self-assembly [21]. Self-assembly can be described as the way a structure builds itself from smaller modular construction units to form an ordered pattern from a disordered state. This process is driven by the interaction among the building blocks rather than the generally stronger bonding force within the particles themselves which in turn is driven by energy minimization towards equilibrium in order to form static structures [22]. The interactions that play an important role are the electrostatic, van der Waals and depletion interactions, and when compiled together they yield a minimum interaction energy that depends on the size and separation of the particles [23, 24].

Earlier research from the PIN group has shown that nanoparticles assemble themselves in interesting ways [23]. When droplets of suspensions containing nanoparticles dry due to evaporation after they have been deposited on a substrate, the result is the well-known coffee-stain ring. This ring is pinned from the moment the droplet comes into contact with the substrate, and particles always assemble near the contact line. When this ring is examined more closely, it turns out that the particles have assembled themselves in ordered domains, where the order depends on the distance to the edge of the ring. Furthermore, in a recent paper it was shown that for micron-sized particles, it is possible to control the spatial extent of the order within the deposits by ultrasonic agitation [25].

This leads to the goal of this thesis, which is to investigate the effect of ultrasonic agitation on nanoparticle ordering within drying deposits. After synthesis of the GNRs, the deposition on SiO_2 and HOPG substrates is investigated using a Scanning Electron Microscope (SEM). The HOPG substrates are also investigated by Atomic Force Microscopy (AFM). These results will then be analyzed in relation to earlier research by taking into account the effective interactions between the nanorods in suspension.

In the reminder of this thesis relevant theory will first be discussed in chapter 2. Chapter 3 contains the experimental aspects and will explain how the measurements were done. The results and discussion can be found in chapter 4, while conclusions are drawn in chapter 5 as well as the recommendations. Chapter 6 has the references that were used for this assignment, and the appendices are found in chapter 7.

2 Theoretical aspects

2.1 Synthesis of GNRs using the seed-mediated growth method

GNRs were synthesized using the seed-mediated growth method described in the paper by Nikoobakht and El-Sayed [18]. In order to synthesize the GNRs, two solutions needed to be prepared; a seed solution and a growth solution. The most important components of the seed solution are colloidal gold nanospheres coated with the surfactant hexadecyltrimethylammoniumbromide (CTAB). These seeds were produced by adding $NaBH_4$ to a solution containing CTAB and $HAuCl_4$. The $NaBH_4$ reacts with the Au^{3+} ions of $HAuCl_4$ to form gold atoms. These atoms will form gold particles, which would normally grow until they agglomerate. However, the present CTAB will attach itself to the forming gold particles, preventing them from becoming bigger than several nanometers.
The growth solution is produced by adding a weak reducing agent (ascorbic acid) to a mixture of $HAuCl_4$, silver nitrate and CTAB. In the presence of CTAB ascorbic acid reacts with the Au^{3+} ions to form Au^{+} ions, but is not strong enough to let gold atoms form [26, 27]. However, in the presence of colloidal gold particles, the Au^{+} ions will react to gold atoms on the surface of the colloidal gold particles. So by mixing the growth solution and the seed solution, the seeds will grow due to the reaction of $HAuCl_4$ and ascorbic acid on its surface.

The size and shape of the seeds that were grown after mixing the solutions, depend on many variables of the growth process. For the seed-mediated growth method, the interesting variables are the size of the seeds [18] and the concentrations of HCl, CTAB and silver nitrate [15]. How these variables influence the process exactly is not completely understood, but the effect of the components is found in several studies and will be discussed below.

2.1.1 Role of seed size

In a paper by Gole et al GNRs were grown using a seed-mediated growth method using seeds of different sizes [28]. Their results indicate that the size of the GNRs depend on the size of the seeds that were used. It was shown that an increase in the size of the seeds results in a decrease of the AR of the GNRs as shown in figure 2.1. Even though the growth method described in this paper does not include silver nitrate, it is expected that the same results hold for growth methods that do use silver nitrate.

2.1.2 Role of CTAB

An influence of CTAB on the shape of the GNRs has been verified in many studies [15, 19, 29, 30]. Adding CTAB to the process increases the stability of the nanoparticles [15] and reduces the reaction speed [19]. By increasing the concentration of CTAB the AR of the GNRs increases [29, 30], which makes choosing the right concentration of CTAB important for getting GNRs with the desired AR.
While it is clear that CTAB has an effect on GNR formation, the effect is not understood completely. Many papers suggest that the CTAB forms a double layer on the surface of the GNRs [15], but there is no definite conclusion about how this effects the growth of GNRs. In order to give some idea of the effect of the CTAB, some theories concerning this effect will be discussed below.

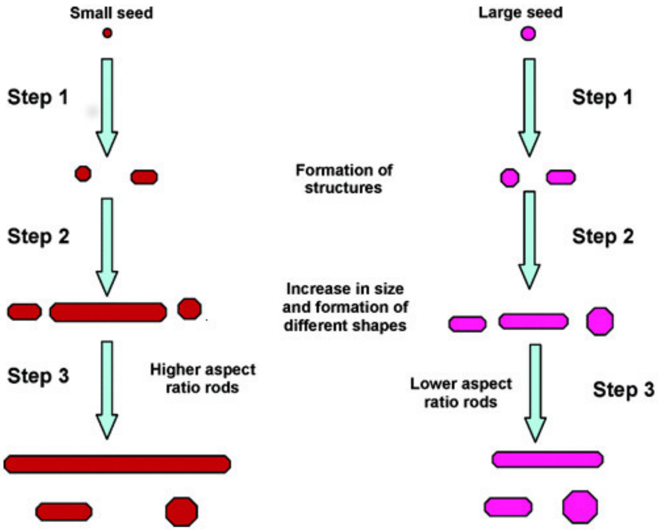

Figure 2.1: This figure shows the different stages of the growth of GNRs using different sizes of seeds. The figure has been modified from the original [28].

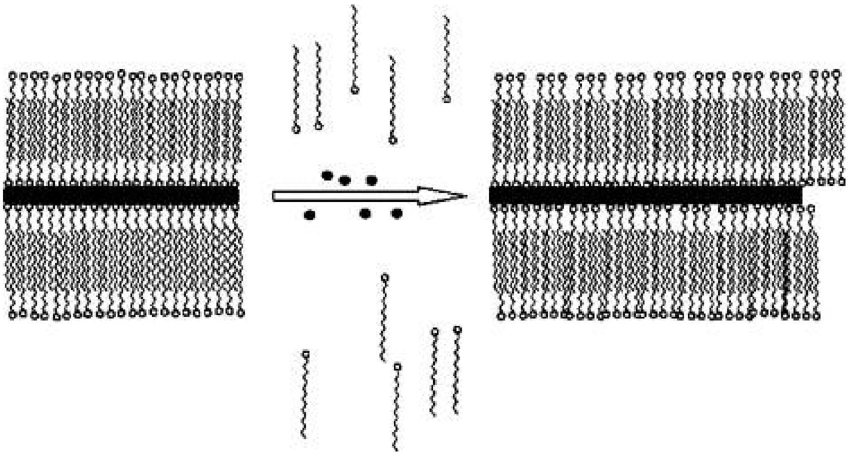

Figure 2.2: A schematic illustration of the zipping procedure of CTAB [15].

The first theory suggests that CTAB has a stronger interaction with the {110} facets at the sides of a GNR than with the {111} and {100} facets at the tips. It is postulated that this stronger interaction with the side facets originates from the higher surface energy of the {110} facets [31]. So due to a denser layer of CTAB on the sides of a GNR, the GNR grows faster along its longitudinal axis. An additional theory about the favorable bonding of CTAB on the side facets is the zipping mechanism. This mechanism is based on the van der Waals interaction between the tails of CTAB and on the preferable bonding of the CTAB with the side facets. It is suggested that the bilayer of CTAB on the side facets extends itself away from the GNR. This again results in preferable growth in the longitudinal direction [32]. Figure 2.2 shows a visualization of this zipping mechanism.

Another theory suggests that the effect originates from the positive charge that GNRs have due to the CTAB bilayer. The Au^{+} ions in the solution are bound to CTAB-micelles, which are positively charged as well. So because CTAB gives both the GNRs and the Au^{+} ions a high positive charge, the interaction between the two is strongly reduced leading to a slower total reaction when CTAB is added. The positive charge also explains the increase in AR since at the tip of a GNR, the surface potential reduces more quickly than at the sides of a GNR. This means that interactions between micelles and GNRs are more likely to occur at the tips of GNRs making longitudinal growth once again more preferable [19].

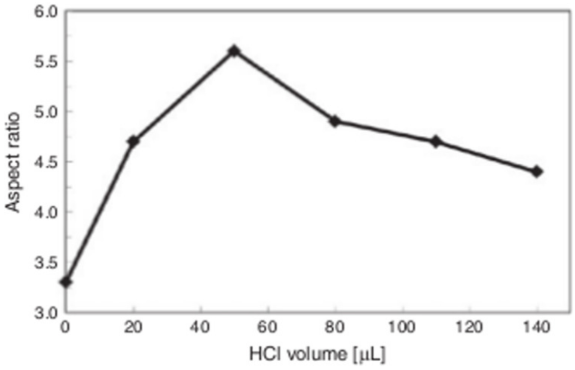

Figure 2.3: This figure shows the effect of adding different amounts of HCl during synthesis on the AR of GNRs [27].

2.1.3 Role of HCl

The reducing ability of ascorbic acid decreases as the pH of the solution decreases. Since adding HCl to a solution reduces the pH, adding HCl decreases the reducing ability of ascorbic acid. That means that adding HCl during the synthesis decreases the speed of the seed growth and increases the AR of the formed GNRs. However, apart from decreasing the reducing ability of ascorbic acid, HCl also etches the sides of GNRs, preferably along the longitudinal axis. At high concentrations of HCl the effect of the etching starts to dominate over the decrease in reducing ability, which then reduces the positive effect of HCl on the AR of GNRs [27].

For different growth methods it has been observed that adding HCl during synthesis can increase the AR of the formed GNRs [27, 28]. For the seed-mediated method it was also observed that adding too much HCl reduces this positive effect on the AR [27]. In research done by Zhang et al, different amounts of HCl were added during the synthesis of several solutions. Their results are shown in figure 2.3 and show that there is indeed an ideal amount of HCl that should be added during the synthesis. For their method of synthesis, the amount was about 40 µL [27].

2.1.4 Role of silver nitrate

Experimental studies show that adding silver nitrate during synthesis increases the yield of GNRs and improves the control over their AR [19]. According to Nikoobakht and El-Sayed the AR of GNRs can be controlled between 1,5 and 5 by adding varying amounts of silver nitrate [18].

Two theories have been proposed of how the silver nitrate influences the growth of GNRs [33, 34]. Some researchers propose that silver bonds to the bromide at the surface of the GNRs. This would mean that the silver ions have the same function as CTAB which is to direct the growth of the GNRs. Other researchers propose that instead of bonding with bromide, the silver forms a (sub)monolayer at the surface of the GNRs. This again induces preferable longitudinal growth due to the preferred growth of silver nitrate on the side facets of the GNRs. XPS measurements have indeed shown a presence of silver at the surface of the GNRs, but were inconclusive about whether its presence was bonded or as a monolayer [8].

2.2 Surface plasmon resonance of metallic nanoparticles

As was mentioned in the introduction, the size and shape of gold nanoparticles affect their optical properties [1–3, 9, 12–16]. This effect is now understood to be due to surface plasmons which have been defined as ‘collective oscillations of conduction band electrons in a metal’ [8] that occur when a particle is exposed to an incident light beam.

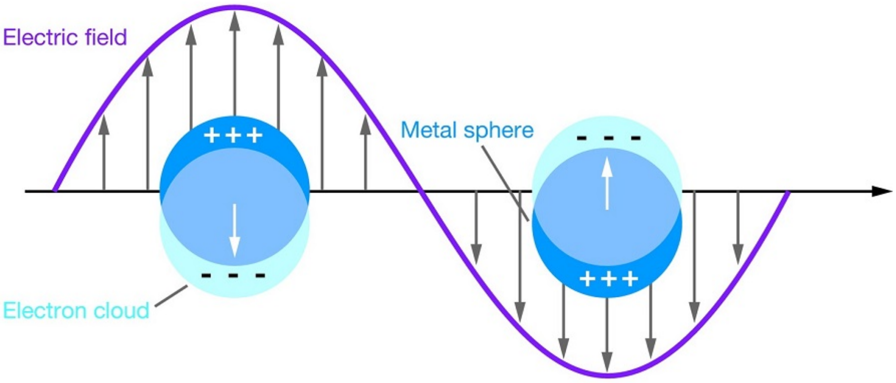

Figure 2.4: A schematic illustration of a localized surface plasmon [35].

A schematic illustration of a light wave causing localized surface plasmons can be seen in figure 2.4. Surface plasmon resonances give rise to a strong optical absorption peak in the extinction spectrum which can be measured using UV-VIS spectroscopy, a technique commonly used for characterization of GNRs and their suspension. When plotting these extinction spectra, the position of the peak is determined by the shape and size of the particles. For ellipsoidal particles, multiple peaks can be observed that correspond to either the transverse or longitudinal resonance mode(s).

The experimental optical extinction spectra are often compared to calculations by using the quasi-static or dipole approximation. Another method is to simulate and analyze the optical properties using the discrete dipole approximation which has all been done earlier in the PIN group [36]. In order to comprehend and simulate the experimental optical extinction spectra and in order to use it to determine the AR of the gold nanoparticles in a solution, a few formulas will be needed that were first provided by Mie [37]. Mie's theory is based on electrodynamics where the resulting extinction efficiency is given by

$$Q_{ext} = \frac{2}{x^2}\sum_{n=1}^{\infty}(2n+1)Re(a_n + b_n) \tag{2.1}$$

where a_n and b_n are the Mie coefficients in terms of the spherical Bessel functions and the size parameter x = ka is a function of the sphere radius a and the wave vector k = $2\pi\sqrt{\epsilon_m}/\lambda$, with $\lambda/\sqrt{\epsilon_m}$ the wavelength in the medium surrounding the particles. The extinction efficiency is made up of two components, and energy conservation provides the following

$$Q_{ext} = Q_{abs} + Q_{sca} \text{ or } \sigma_{ext} = \sigma_{abs} + \sigma_{sca}, \tag{2.2}$$

since the efficiencies Q are equal to the cross sections σ, normalized to the (effective) particle cross section πa^2. If the particles are much smaller than the wavelength of the light, the optical properties can be described by just looking at the n=1 term in equation 2.1. The absorption and scattering cross sections are then given by

$$\sigma_{abs} = k\ Im(\alpha) \tag{2.3}$$

$$\sigma_{sca} = \frac{k^4}{6\pi}|\alpha|^2 \tag{2.4}$$

where α is the single particle polarisability. For spherical particles, α is equal to

$$\alpha_{sphere} = 4\pi a^3\frac{\varepsilon_{Au} - \varepsilon_m}{\varepsilon_{Au} + 2\varepsilon_m} \tag{2.5}$$

where a is the radius of the sphere and ε_{Au} and ε_m are the dielectric functions of gold and the host medium respectively. Using equation 2.2, the extinction efficiency can be deduced.

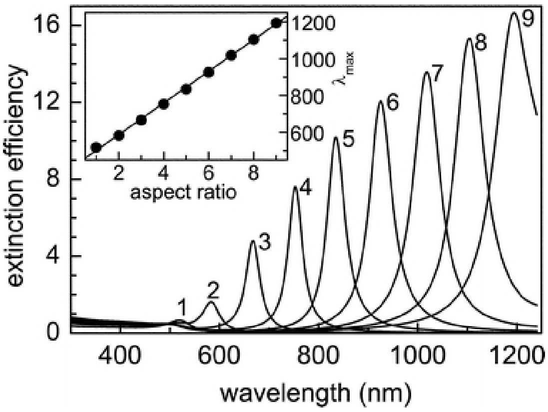

Figure 2.5: Optical extinction spectra of ellipsoidal gold nanoparticles calculated using the quasi-static approximation. The ellipsoids have a short radius *b* = 5 nm and the long radius *a* varies from 5 nm (a sphere) to 45 nm, corresponding to ARs 1-9 as indicated. The inset shows the position of the longitudinal plasmon resonance peak as a function of AR [36].

Mie theory however, is not valid for non-spherical particles so in order to calculate the optical properties of GNRs, Gans theory is used. This is an extension of the Mie theory that introduces depolarization factors for each direction in the expressions in order to compensate for the optical anisotropy. The depolarization factor for an ellipsoid along it's long axis is given by

$$L = \frac{1-e^2}{e^2}\left(\frac{1}{2e}ln\left(\frac{1+e}{1-e}\right)-1\right) \tag{2.6}$$

where e is the eccentricity $e = \sqrt{1-1/\eta^2}$ and η is the AR defined as the long radius a divided by the short radius b of an ellipsoidal particle. Introducing this depolarization factor in equation 2.5 gives

$$\alpha_{ellipsoid} = \frac{4\pi}{3}ab^2\frac{\varepsilon_{Au}-\varepsilon_m}{\varepsilon_m+L(\varepsilon_{Au}-\varepsilon_m)} \tag{2.7}$$

since inserting $a = b$ and L = 1/3 gives equation 2.5 for a spherical particle.

In this theory, the optical properties are only dependent on the AR of the GNRs, not on the absolute dimensions. Furthermore it predicts that for particles smaller than the wavelength of the light, the plasmon mode will split into two distinct modes; the longitudinal and transverse modes. Even though GNRs are more cylinder-shaped, Gans theory does match experimental data in most cases [38].

These theories and earlier work from the PIN group [36] are used to interpret and simulate the extinction spectra that were found using UV-VIS spectroscopy.

Figure 2.5 shows the optical extinction spectra that were determined by PIN using the quasi-static approximation. The extinction efficiency Q_{ext} is plotted as a function of the wavelength for ARs 1-9. This information can be used to determine the AR of the GNRs in different solutions. Furthermore, knowing the extinction efficiency also made it was possible to calculate the density of GNRs and nanospheres in the solutions that were used. Even though this is a good method to base this assignment on, it has to be mentioned that it remains an approximation that is based on the AR of the nanoparticles. It does not take into account the actual dimensions, even though the peak position for fixed AR moves to longer wavelengths for increasing dimensions of the ellipsoidal particles [36].

Something else that should be kept in mind, is the fact that the solutions that were made do not only contain GNRs of one AR, but instead will be a mixture of different ARs. Furthermore, the concentrations of different ARs in the solutions will probably follow a normal distribution. The result is that the peaks from the approximation will shift to the right, indicating that the ARs of the GNRs are larger than they should be since GNRs with higher ARs have a contribute more than GNRs with lower ARs.

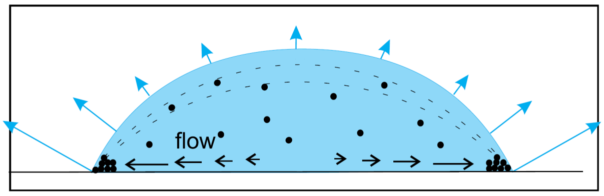

Figure 2.6: An evaporating droplet with the contact line pinned on the surface. The arrows above the droplet represent the evaporation flux which diverges at the contact line. The flow of liquid to compensate for the evaporated liquid from the edge is represented with the arrows inside the droplet. This flow brings the dispersed particles to the edge forming the coffee-stain ring at the end of the evaporation [53].

2.3 Ultrasonic agitation

In order to vibrate the substrate containing the evaporating droplet of a solution with gold nanoparticles, ultrasonic agitation was used. The ultrasound spectrum consists of frequencies beyond the hearing range of the human ear, ranging from 20 kHz to several MHz. This range of frequencies can cause oscillating sound waves within a liquid which in turn trigger a process called acoustic cavitation. This is defined as ‘the formation, growth and collapse of microbubbles within an aqueous solution’ [39]. When a bubble collapses, a microscopic implosion occurs with high local turbulence where pressures can increase up to several hundred Bar. The local temperature can also significantly increase to several thousand degrees Kelvin resulting in a release of heat energy. These strong disturbances generate shock waves, microstreamers and microjets which lead to mechanical effects like mixing and shearing. This effect is greatest at frequencies up to 100 kHz since the generated bubbles are relatively large, resulting in strong shockwaves when they collapse [40].

These significant effects at microscopic scales can be used for various applications including enhancing chemical processes [41], emulsifying oils [42] and for the degradation of chemical or biological pollutants [43]. For this thesis, ultrasonic agitation is used for it’s mechanical effects since it could facilitate mass transport in the droplet as it evaporates on the sample. Results of experiments by Lash et al. suggest that ultrasonic agitation creates convective fluidic motion that may encourage macroscopic motion of particles as well as interparticle collisions [25]. It has also been shown that ultrasonic agitation can be used to induce the close packing of particles in 3D structures [44,45].

2.4 Deposition and self-assembly of gold nanoparticles on a substrate

The shape [46,47] and size [48,49] of gold nanoparticles, the evaporation rate [17,50] of the droplet and particle interactions [17,48,49,51,52] have an influence on the way they self-assemble on a substrate. Furthermore, the deposition of particles also depends on the substrate since it can have an influence on droplet drying during the evaporation process.

2.4.1 Assembly on silicon dioxide (SiO_2)

In general, SiO_2 wafers are widely used in semiconductor manufacturing and thin film research. Wafers can easily be diced into smaller pieces and can be used directly in SEM and AFM imaging. Next to that, the surface is very flat making it suitable for the deposition and research of droplets containing nanoparticles.

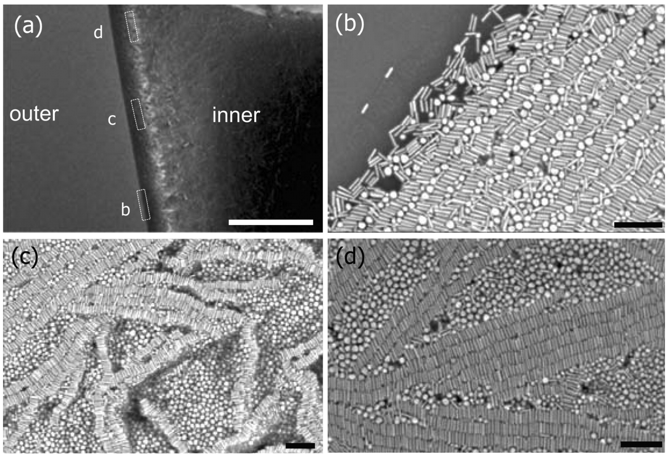

Figure 2.7: SEM images at different positions on the coffee-stain ring. (a) A large scale overview (scale bar is 20 µm). (b) The outer edge of the ring and the three-phase contact line. (c) 4-6 µm from the contact line. (d) 6-10 µm from the contact line. The scale bars in b-d are 200 nm [23].

The evaporation process of a droplet on a hydrophilic surface

When a droplet is deposited on an SiO_2 substrate, evaporation of the solvent typically takes about 1-2 hours. The result is a coffee-stain ring in which all the nanoparticles that were first dispersed in the whole droplet seem to be concentrated in the outer ring. This effect is ascribed to convective processes that occur while the droplet evaporates. [54–57]. When the contact line is pinned, which is what happens on hydrophilic surfaces [53], the fluid flows outwards to compensate for evaporative losses. This capillary flow plays an important role since it ensures that liquid evaporating from the edge is replenished by liquid from the interior. The outward flow carries almost all dispersed particles to the edge of the ring [58]. An illustration of this process can be found in figure 2.6.

Self-assembly of GNRs

It has been shown that GNRs have a strong preference to assemble side-by-side, forming smectic phases [23]. If the deposited droplet also contains gold nanospheres, these particles are forced out of regions with a high density of GNRs and form close-packed arrays elsewhere. This self-assembly has been observed many times [59–62] and has been shown to be related to several interactions including electrostatic, van der Waals and depletion interaction forces. These interactions are regulated by the fundamental concept that a system will always deform or displace to the position in which its energy is at a minimum. Furthermore the surfactant that was used for synthesis could also have an influence on assembly since the nanoparticles are covered by a bilayer of surfactant [23].

According to earlier research from the PIN group [23], the observed coffee-stain ring can be divided into three regions where different assemblies are observed. The first is the most outer part of the ring from the three-phase contact line until about 3 or 4 µm inward. At the three-phase contact line, only GNRs can be found that are assembled parallel to the contact line. A couple nanorod-lengths further inward, the rods are oriented perpendicular to the contact line and are assembled in a side-by-side manner. These rows of GNRs are alternated by rows of single gold nanospheres (see figure 2.7b). The next region is located about 4 to 6 µm from the contact line. Here, randomly oriented 3D superstructures are observed, with chains of side-by-side assembled GNRs and regions with closely packed gold nanospheres (see figure 2.7c). In the last region, about 6 to 10 µm from the contact line, the phase separation is most pronounced. Large chains of GNRs are assembled together into 3D structures without containing any gold nanospheres. The gold nanospheres also aggregate into large groups of closely packed particles, but in some places GNRs can still be found (see figure 2.7d).

Furthermore, the different energy contributions (electrostatic, van der Waals and depletion), which depend on the diameter and length of the rods, were calculated.

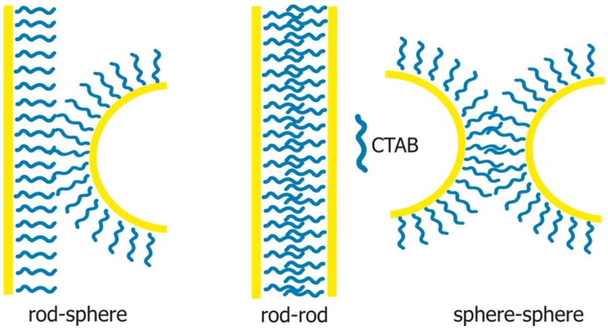

Figure 2.9: A schematic drawing of the surfactant at different curved surfaces. The interaction between a flat and curved surface (left), two flat surfaces (middle) and two curved surfaces (right) is shown [23].

The result of this calculation can be found in figure 2.8, where the electrostatic, van der Waals and depletion interaction curves are plotted along with the sum of all the individual contributions, i.e. the total interaction curve. It was shown that the side-by-side assembly of GNRs is indeed favorable since the total interaction curve was more negative than kT (the energy related to Brownian motion). For GNRs with relatively large ARs, this outcome is due to the fact that the van der Waals forces between the long edges of the GNRs are much larger than the van der Waals forces between the ends of the GNRs, which would have resulted in end-to-end assembly [24].

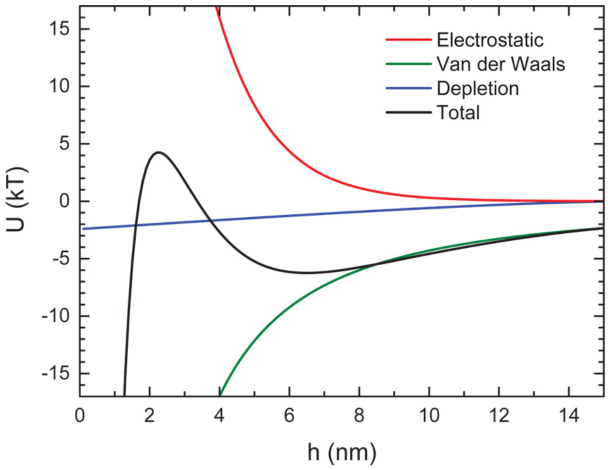

Figure 2.8: Theoretical curves for the electrostatic (red), van der Waals (green) and depletion (blue) interactions for side-by-side aligned GNRs with a length of 60 nm and diameter of 10 nm. The total interaction curve (black) is the sum of all individual contributions [23].

The fact that different regions occur in the assembly of nanoparticles can be explained by the evaporation process of the droplet. At the edge of the ring well-ordered structures are observed because in the beginning of the evaporation of a droplet, the speed is low and the nanoparticles have enough time to arrange themselves. At a later stage in the evaporation process, a rise in the evaporation rate of the droplet causes a sharp increase in the arrival of nanoparticles. As a result the particles no longer have enough time to assemble themselves and thus creating different structures [53, 57].

Lastly the role of CTAB (the surfactant) was also discussed. It was shown that it could also play a role in the self-assembly process, since the interaction between a flat surface and a curved surface (of the particles) is less favorable than an interaction between two flat or two curved surfaces since in the first case the orientation of the tails of the CTAB molecules mismatch, giving rise to repulsion. A schematic drawing of this can be found in figure 2.9.

2.4.2 Assembly on Highly Ordered Pyrolytic Graphite (HOPG)

Highly ordered Pyrolytic Graphite (HOPG) is a very pure form of carbon that has a very smooth surface due to its lamellar structure. The forces within the lateral planes are much stronger than the forces between the planes, making it very suitable to cleave with ordinary tape to create a clean and smooth result. Additionally, the surface of HOPG is hydrophobic.

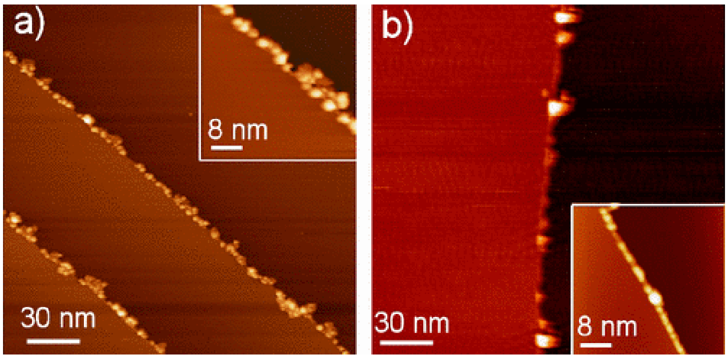

Figure 2.10: STM images (200X200 nm^2) of HOPG with Fe nanoparticles decorating the step edges. (a) Fe nanoparticles on HOPG as deposited, (b) Fe nanoparticles on HOPG after annealing at 900 °C without methane in ultra-high vacuum conditions. The insets show a higher magnification of the images (40X40 nm^2). The thermal treatment without methane does not alter the HOPG step edges [63].

The evaporation process of a droplet on a hydrophobic surface

The evaportation process of a droplet on HOPG is the same as on SiO_2, except for the fact that the contact line does not stay pinned from the moment the droplet is on the substrate due to its hydrophobicity. This means that the contact line will jump as the droplet evaporates, also referred to as stick-slip motion, leaving a ring of particles behind each time [53].

Assembly

At this point in time, nothing about the evaporative assembly of gold nanoparticles on HOPG samples can be found in literature.

What can be found, that relates to the assembly of nanoparticles on HOPG substrates, is the work done by Kholmanov et al [63]. Their goal was to grow curved graphene sheets on HOPG by chemical vapor deposition at low temperatures using Fe catalytic nanoparticles. The first step of this process was the deposition of Fe nanoparticles using a high-voltage e-beam sublimator to deposit a thin layer. This low coverage had the effect that Fe nanoparticles preferably decorated the step edges of the topmost graphene layers while the terraces remained almost completely uncovered. Figure 2.10 shows STM images of the HOPG samples with decorated step edges where it can clearly be seen that Fe nanoparticles align along the step edges and the HOPG terraces remain empty.

Something else that is related to self-assembly on HOPG substrates is the work by Shimonaka et al [64]. In their work, the forming of Ge nanostructures on HOPG surfaces was investigated under various conditions like different temperatures and deposition amounts. The experiments were carried out in a chamber with ultrahigh vacuum with an in situ Knudsen cell for the deposition of Ge and an in situ scanning electron microscope (SEM) to analyze the substrates. Ge was deposited at various temperatures and in various amounts at a rate of 0,24 nm/min. Figure 2.11 shows SEM images of the HOPG samples with Ge clusters clearly formed at the step edges on HOPG for various temperatures.

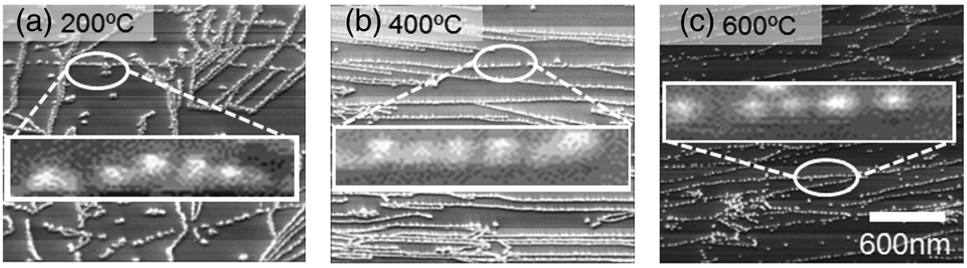

Figure 2.11: SEM images of Ge clusters after 5 nm of Ge was deposited at (a) 200, (b) 400, and (c) 600 °C. The white rectangels are enlarged images of the corresponding regions [64].

3 Experimental aspects and measurements

3.1 Synthesis of GNRs using the seed-mediated growth method

For the synthesis of the GNRs the following materials were used: cetyltrimethylammonium bromide (CTAB, Aldrich, 99%), Hydrogen tetrachloroaurate ($HAuCl_4 \cdot 3H_2O$, 99,999%, Aldrich), silver nitrate ($AgNO_3$, Acros), ascorbic acid (AA, 99%, Merck), sodium borohydrate ($NaBH_4$, 99%, Aldrich), and hydrochloric acid (HCl, 37%, Merck). The water used during the synthesis had a Milli-Q quality (18.2 $M\Omega$cm) and was produced with a Milli-Q Reference system (Millipore).

GNRs were synthesized using the seed-mediated growth method described in a paper by Nikoobakht and El-Sayed [18]. The seed solution was prepared by first adding 25 µL of 0,1 M $HAuCl_4$ to 10 mL of 0,1 M CTAB after which the solution was stirred. Next, while still stirring the solution, 60 µL of ice cold 0,1 M $NaBH_4$ was added. The solution was stirred for 3 minutes and then left undisturbed for at least 30 minutes at 25 ^oC.
Six different GNR solutions were prepared to produce GNRs of different ARs. A solution made by the PIN group was used as a reference. The chemicals and their volumes and concentrations used in the production of this reference solution are listed in the upper half of table 3.1. The solution was produced by first mixing the CTAB with the $HAuCl_4$ followed by adding the $AgNO_3$. Next the ascorbic acid was added, after which the solution was stirred till it was colorless. The HCl was added next and lastly the seed solution was added, while stirring the solution vigorously. The solution was then left undisturbed for one day to give the reaction time to finish. The six different solutions were produced by following the process of the reference solution while changing the volume of one of the used chemicals. The chemicals that were altered for each solution are listed in the lower half of table 3.1.

After synthesis a lot of excessive CTAB and other chemicals that were no longer necessary remained

Chemicals	Volume	Concentration
CTAB	10 mL	0,1 M
$HAuCl_4$	50 µL	0,1 M
$AgNo_3$	15 µL	0,1 M
Ascorbic acid	70 µL	0,1 M
HCl	50 µL	1 M
Seed solution	24 µL	-

Solution	Chemicals that were altered	New volume
1	HCl	50 µL
2	HCl	200 µL
3	$AgNo_3$	25 µL
4	$AgNo_3$	50 µL
5	$AgNo_3$	8 µL
6	$AgNo_3$	12 µL

Table 3.1: The upper half of the table shows the recipe of the reference solution while the lower half of the table shows the modifications made in the solutions that were produced.

dissolved in the solutions. In order to separate the GNRs from these excessive chemicals, centrifugation was used. The solutions were put in a Hermle high-speed centrifuge Z36 HK, which was set at 15000 rpm for 10 minutes. This caused all the GNRs to sink to the bottom of the test tubes while CTAB and other chemicals remained dissolved in the water. The water was then removed as well as possible by carefully pouring it out, leaving the layer of GNRs behind. The remaining highly concentrated solution of GNRs was then diluted to approximately its original concentration by adding water. The centrifugation process was then repeated once more to further purify the GNRs solution.

3.2 Deposition and assembly

GNRs were deposited by letting a droplet evaporate on a substrate. GNRs of two different solutions were deposited. The first solution was a solution containing mostly GNRs and almost no gold nanospheres and the second solution was a solution provided by the PIN group containing both gold nanospheres and GNRs. On four different substrates a droplet of both solutions was deposited. Two of the substrates were CZ-silicon wafers (Okmetic, p-type doped with Boron, orientation (100), cleaned with ethanol and dried with N_2 gas) and the other two substrates were highly ordered pyrolytic graphite (HOPG of SPI-2 grade, SPI Supplies, mosaic angle 0,8 ° +/- 0,2 °, cleaved with regular tape, cleaned with ethanol and dried with N_2 gas). One of the silicon substrates and one of the HOPG substrates was left undisturbed during the evaporation process. The other two substrates were ultrasonically agitated at a frequency of 60 kHz during the evaporation process. This ultrasonic agitation was induced by placing the substrate on a Petri dish floating in a HBM 2,5 Liter Ultrasonic Cleaner filled with water until the droplet was completely evaporated.

3.3 Characterization

3.3.1 UV-VIS Spectroscopy (UV-VIS)

In order to measure the absorption spectra of the solutions containing GNRs, an Ocean Optics HR200+ spectrometer along with a Mikropack UV-vis light source (model DH-2000-BAL) was used operated using the SpectraSuite software package. With this set-up, spectra with wavelengths ranging from 400 nm to 1100 nm were measured. The outer dimensions of the cuvettes that were used to contain the liquids as they were being analyzed were 12,5 mm x 12,5 mm x 45 mm, holding up to 1,5 mL of liquid.

3.3.2 Scanning electron microscope (SEM)

For the imaging of the substrates, a high-resolution scanning electron microscope (SEM, a Mirlin Zeiss 1550 system) was used. This SEM has an ultimate resolution of the order of 1 nm.

3.3.3 Atomic force microscopy (AFM)

An atomic force microscope (AFM, Agilent s100) in tapping mode was also used to analyze the substrates in combination with HQ: NSC35/Al probes (Micromash) with a nominal spring constant of 5-16N/m and a resonance frequency of 150-300 KHz.

4 Results and discussion

4.1 Aspect ratio of GNRs

During synthesis, the concentrations of HCl and silver nitrate were varied to produce solutions with different ratios of GNRs versus gold nanospheres. Figure 4.1 shows the absorption spectra of these solutions. For the deposition on the substrates a solution with (almost) only GNRs and a solution with both GNRs and gold nanospheres were needed. Solution 1 was used as the solution with (almost) only GNRs, since its absorption spectrum had a high longitudinal peak and a low transverse peak indicating a low concentration of gold nanospheres. This solution also had a nice absorption spectrum which made is easier to estimate its AR using simulations. For the solution with GNRs and gold nanospheres a solution from the research group PIN was used, of which the absorption spectrum can be found in figure 4.2. The ratio of GNRs versus gold nanospheres in this solution is much higher than the ratios of solutions that were produced due to its relatively high transverse peak.

The ARs of the GNRs in solution 1 and in solution PIN have been estimated by comparing their absorption spectra with absorption spectra that were simulated based on the quasi-static approximation (also used to simulate the spectra in figure 2.5). For this simulation a normal distribution for the ARs of the GNRs is assumed since the solutions do not contain GNRs with only one AR. These simulated absorption spectra are plotted for both solutions together with the original spectra in figure 4.2. The ARs used for the simulation are shown in the first column of table 4.1. More details about the relation between the longitudinal peak position and the distribution of the AR of the GNRs can be found in Appendix B.

The ARs of solution 1 and solution PIN were also evaluated by measuring the length and width of GNRs in the SEM images, made of the deposited droplets (for example: figure 4.4). Only GNRs near the outer edge in clear mono-layers were measured to be sure that none of the measured GNRs were tilted. If tilted GNRs would have been measured, the measured lengths and/or widths would be smaller than the real lengths and widths inducing an error in the measurements. The ARs of the GNRs were calculated using the measured lengths and widths. The distributions of these ARs are presented in the histograms in figure 4.3 and they show that solution PIN indeed has relatively more gold nanospheres than solution 1. By taking the average of the data in the histograms, an estimate of the ARs of GNRs in solution 1 and solution PIN has been made. ARs lower than two were left out of this calculation since they resemble the gold nanospheres in the solutions. The calculated ARs can be found in the second column of table 4.1.

Comparing the two columns in table 4.1 shows that the two methods that were used to estimate the ARs do not give the same results. For both solutions the ARs estimated by simulating the absorption spectra are higher than those estimated from the histograms. While the ARs estimated from the histograms are almost equal for both solutions, the ARs estimated by simulating the absorption spectra are

	ARs from the absorption spectra	ARs from the histograms
Solution of PIN	6,5 ±1,6	4,6
Solution 1	5,2 ±1,4	4,4

Table 4.1: The ARs of the GNRs in solution 1 and solution PIN. The ARs in the first column were estimated using the simulations from figure 4.2 and represent the 95% intervals of the normal distributions. The ARs in the second column were estimated using the histograms in figure 4.3.

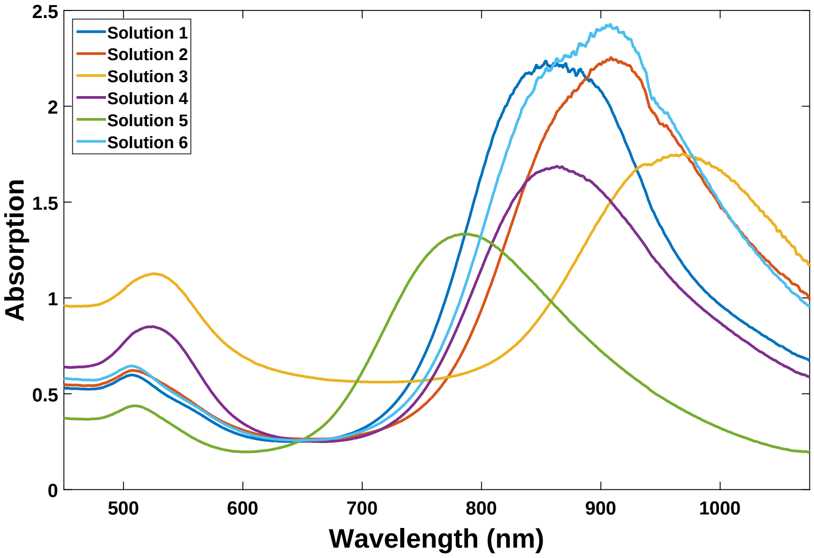

Figure 4.1: The absorption spectra of the six solutions that were produced. The numbering in the legend corresponds to the numbering in table 3.1.

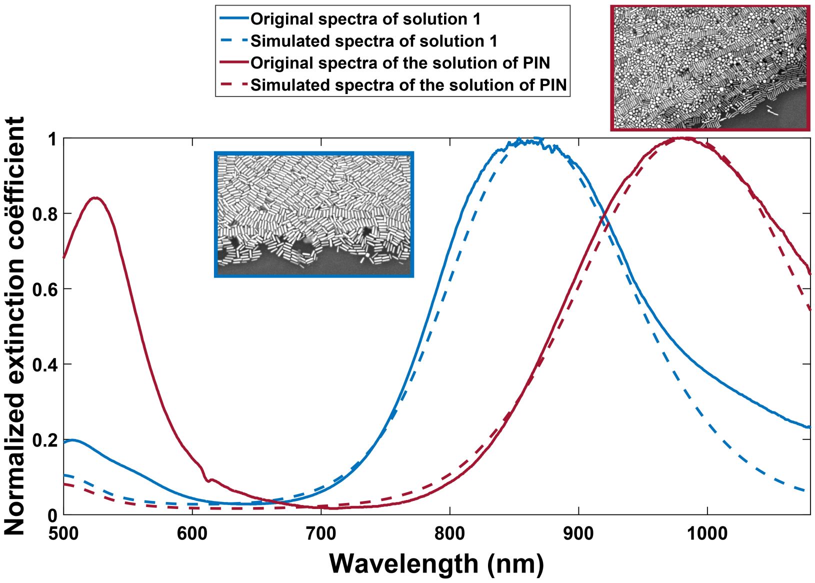

Figure 4.2: The original and simulated absorption spectra of solution 1 (blue) and the original and simulated absorption spectra of the solution PIN (red). The extinction coefficient is normalized to show the resemblances more clearly.

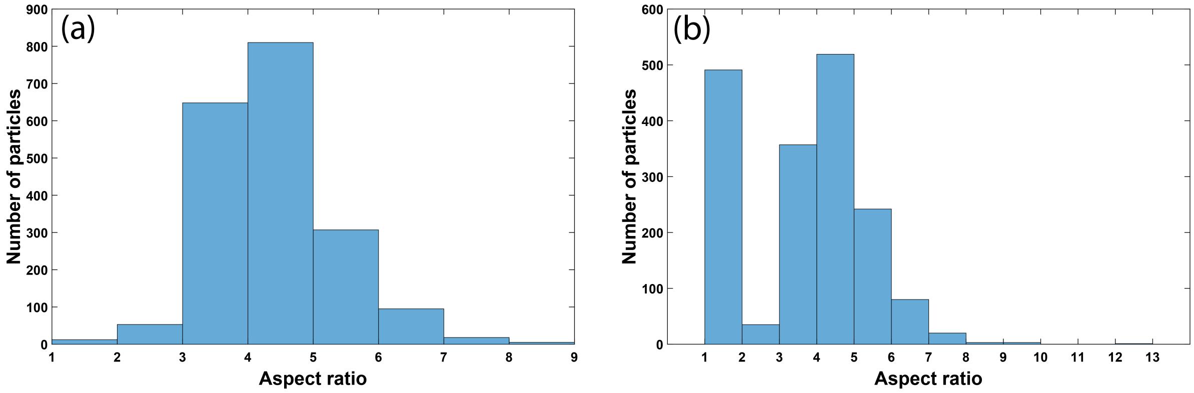

Figure 4.3: Histograms of the ARs that were measured by measuring the length and width of GNRs in SEM images. (a) shows a histogram of the ARs of solution 1, while (b) shows a histogram of the ARs of solution PIN.

very different. There are several possible explanations for this deviation. Firstly, in the SEM images only GNRs at the three-phase contact line of the droplet were measured. So if GNRs with high ARs prefer to assemble away from this contact line, they were not measured. Secondly, in the calculation used for the simulation it is assumed that the volume of the GNRs have no effect on the position of the longitudinal peak, while the position of this peak does increase with increasing volume. This could be the explanation for the difference between the two methods of estimating the ARs of the GNRs. If GNRs in solution PIN had a higher volume as compared to GNRs in solution 1, the not included volume dependence would also explain the big difference between the estimated ARs by simulating the absorption spectra. The SEM images and data used for the histograms show however, that the volume of the nanoparticles in the two solutions is not different.

4.2 General discussion

Before the results can be analyzed and discussed, it is important to keep in mind that a lot of factors play a role when it comes to the evaporation of the droplets and the deposition of the coffee-stain ring on both the SiO_2 and HOPG substrates. Factors like surface-tension gradients, solute diffusion, and electrostatic and gravity effects are negligible during evaporation [58], but the temperature during evaporation, the humidity and the air flow around the substrates are not. During the experiments these factors were not controlled, so it's possible that they had an unwanted or unexpected influence on the outcome of the experiments.

For example, the temperature of the bath that was used to ultrasonically agitate the droplets on the substrates rose over 10 °C. This relatively big increase in the temperature of the bath probably caused the substrate itself to increase in temperature, which could have increased the thermal vibrations of the particles in the droplet and also increased the evaporation rate of the droplet itself. The surroundings of the substrate that was left undisturbed did not increase in temperature. Since there was probably also an increase in humidity in the air surrounding the agitated substrates due to the fact they were surrounded by water, that may then have slowed the evaporation rate of the agitated droplets.

Two factors that were kept constant are the mass of the particles and the concentrations of the solutions. Considering that all GNRs and gold nanospheres have about equal volumes, their masses are approximately the same. Moreover the concentration of GNRs in solution 1, and the concentrations of both GNRs and gold nanospheres in solution PIN were calculated. These calculations can be found in appendix A. The concentration of GNRs in solution 1 is 5,34 $\times$ 10^{10} per cm^3, while the concentration of GNRs in solution PIN was 1,40 $\times$ 10^{10} per cm^3. The concentration of gold nanospheres in solution PIN was 1,22 $\times$ 10^{11} per cm^3, making the ratio of gold nanospheres to GNRs about 8,7 to 1 which is not a significant difference.

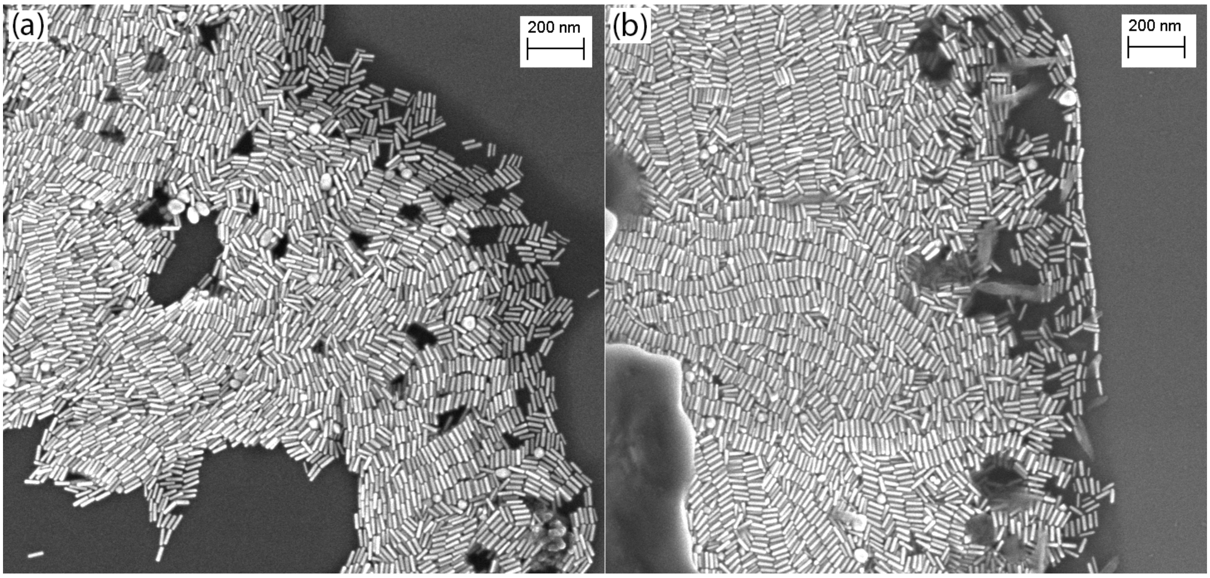

Figure 4.4: Typical SEM images of an evaporated droplet of solution R on a SiO_2 substrate without ultrasonic agitation (a) and with ultrasonic agitation (b).

4.3 Deposition on silicon

As was mentioned in the previous chapter, two solutions were deposited on substrates and studied for this thesis namely solution 1 and the solution from PIN. From this point on, solution 1 will be referred to as solution R since this solution contains mostly GNRs. The solution from PIN will be referred to as solution RS since it contains both GNRs and gold nanospheres. What is observed in all cases is that the result of droplet evaporation is a coffee-stain ring in which all the nanoparticles are concentrated in the outer ring.

4.3.1 Solution R

A droplet of solution R was placed on two SiO_2 substrates; one that was left to dry undisturbed (figure 4.4a) while the other was subjected to ultrasonic agitation (figure 4.4b). Figure 4.4 shows SEM images of similar parts of the three-phase contact line, i.e. the edge of the coffee-stain ring where multilayers of particles can be seen. In both cases, GNRs seem to have a preference of assembling in a side-by-side manner, as was described in chapter 2. End-to-end alignment is extremely rare but can sometimes be seen in the monolayers at the very edge of the ring as in figure 4.4b, where it seems that GNRs prefer to align parallel to the edge of the ring.

There are differences too however. In the case of no ultrasonic agitation, there seems to be some degree of order since most of the GNRs are assembled side-by-side, forming somewhat long chains of assembled particles. Still, this degree of order seems to be much higher in the case of ultrasonic agitation as can be seen in figure 4.4b, since the chains of side-by-side assembled GNRs seem to be longer.

That the chains seem longer in figure 4.4b has also been analyzed quantitatively by measuring the length of each chain in all SEM images for both substrates. The results can be found in figure 4.5a and b, which show histograms of the collected data for the substrate that was not ultrasonically agitated and for the substrate that was ultrasonically agitated respectively. It is easy to see that the chains in figure 4.5a are indeed shorter with an average chain length of about 138 nm. For the substrate that was ultrasonically agitated, the average chain length is 234 nm. So with the ultrasonic agitation there seems to be an increase in the ordering of the assembly of GNRs on SiO_2 substrates.

Assuming the higher degree of order is caused by the ultrasonic agitation suggests that during the evaporation of the droplet the shock waves, caused by the agitation, somehow give the GNRs the

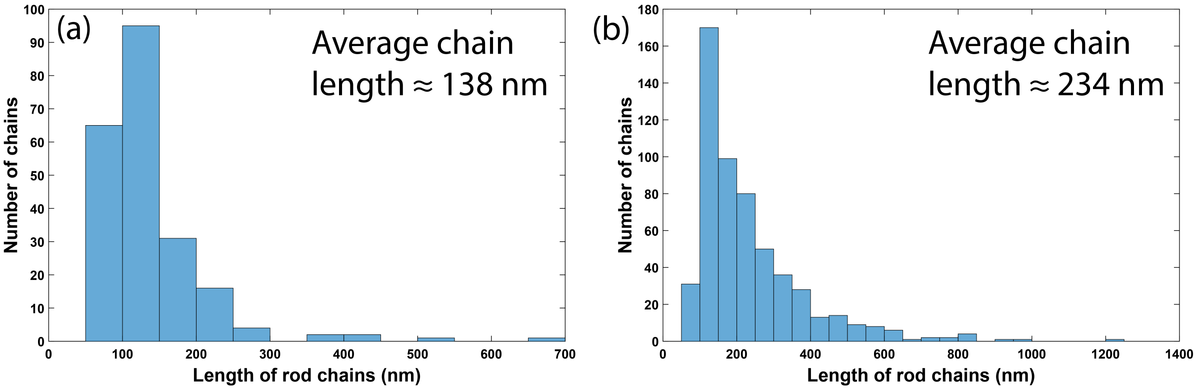

Figure 4.5: Histograms showing the lengths of the chains that were measured. (a) shows collected data for the substrate that was not agitated ultrasonically, (b) shows the collected data for the substrate that was agitated ultrasonically.

chance to find a more favorable position. However, we expect the shock waves to result in more and stronger collisions between superstructures in the droplet. One would expect these collisions to break or deform the superstructures, which would result in a more chaotic deposition with smaller chains. The opposite however, less chaos with longer chains, is observed.
The rise in temperature is a more likely cause of the higher order in the deposition with ultrasonic agitation. As earlier mentioned the temperature rose over 10 degrees during this part of the experiment, increasing the thermal energy of the particles. This extra energy increases the vibration of the GNRs, which could have given them the opportunity to better find their most favourable position.

4.3.2 Solution RS

Figure 4.6 are SEM images taken of the substrates with droplet RS, the droplet containing both GNRs and gold nanospheres. Figure 4.6a and b show the edge of the coffee stain ring of the substrate that was not subjected to ultrasonic agitation, while figure 4.6c and d show a similar edge but of the substrate that was subjected to ultrasonic agitation. In the overview in figure 4.6a it can be seen that the coffee-stain ring consists of two different regions and that in both images there is a very clear phase separation between GNRs and gold nanospheres. In the most outer part of the ring until about 2 µm inward in this image, long chains of side-by-side assembled GNRs are observed laying parallel to the edge of the ring, interspersed by regions of spheres. This can be seen more clearly in figure 4.6b. From about 2 µm from the edge of the ring in figure 4.6a, a different assembly can be observed. Here the long chains of GNRs are no longer aligned parallel to the edge of the ring, and in some cases they are assembled next to each other instead of being interspersed by spheres. Since different regions are observed in the coffee-stain ring and a clear phase separation can be seen, the above is in agreement with earlier research described in chapter two.

The overview in figure 4.6c is very different than figure 4.6a. The phase separation between GNRs and gold nanospheres is taken to an extreme since it can be seen that most of the spheres have disappeared from the edge of the ring. Some of the GNRs are still assembled side-by-side in long chains which are mostly aligned parallel to the edge, while a lot of short chains and loose GNRs are also observed. Generally, the chains of assembled GNRs seem to be much shorter. Figure 4.6d shows more details of the coffee-stain ring where once again the gold nanospheres seem to be absent while the GNRs are assembled side-by-side in shorter chains than in the case of no ultrasonic agitation. The loose GNRs and shorter chains can be observed more clearly here.

Equivalently to solution R, the lengths of the chains of GNRs were measured for solution RS by analyzing the SEM images. Figure 4.8a and 4.8b show the collected data for the substrate that was not ultrasonically agitated and the substrate that was ultrasonically agitated respectively. Since the chains in the case of no ultrasonic agitation are indeed longer than the case with ultrasonic agitation (473 nm vs 302 nm), this supports the observation in the previous paragraph. Furthermore, the insets show a larger image of the data in the histograms for chain lengths of 1000 nm and higher, clearly showing

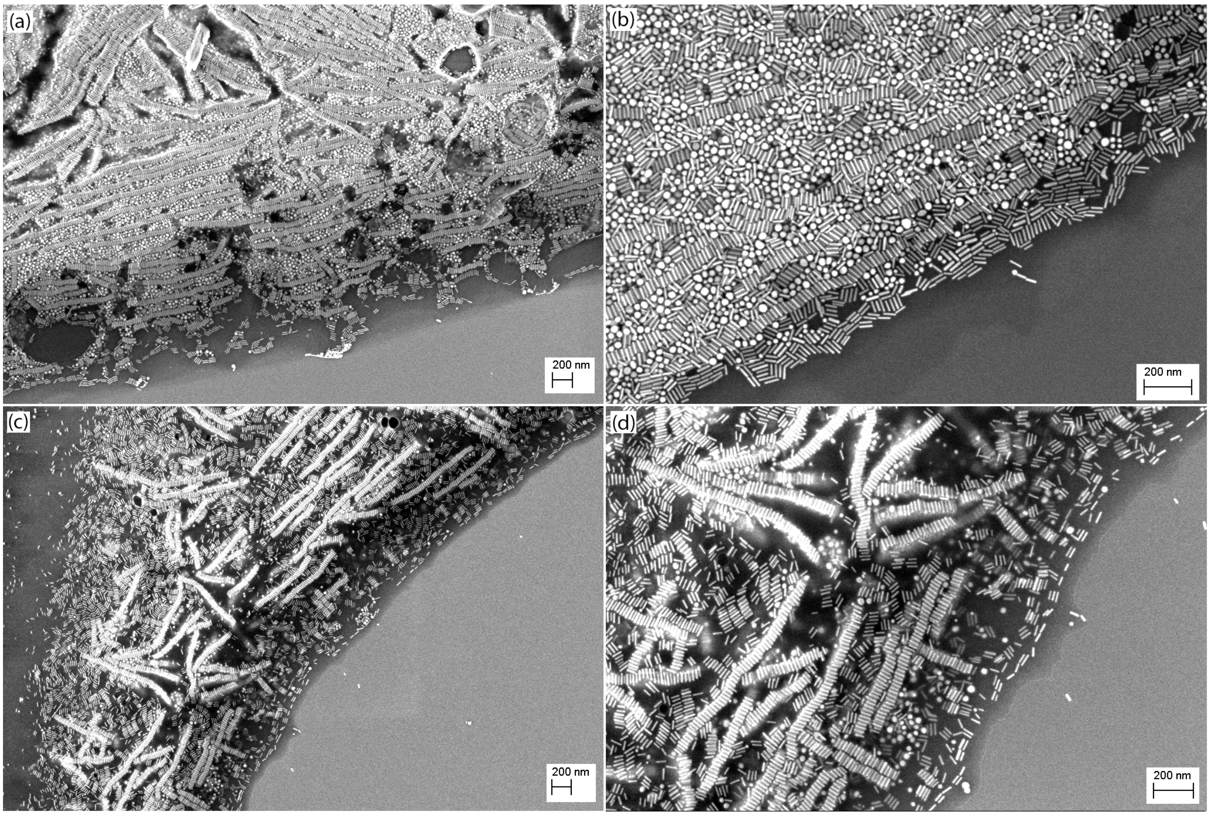

Figure 4.6: Typical SEM images of an evaporated droplet of solution RS on a SiO_2 substrate without ultrasonic agitation (a) and (b) and with ultrasonic agitation (c) and (d).

that the maximum length of the chains for the case of no ultrasonic agitation is much larger than the maximum length of the chains in the other case, again supporting earlier observations.

Something else that stands out when comparing figures 4.6c and 4.6d to figures 4.6a and 4.6b is that the regions that were observed in figures 4.6a and 4.6b look very different in figures 4.6c and 4.6d. In fact, only one region is observed in figures 4.6c and 4.6d as described in the previous paragraph. At about 2µm from the edge of the ring, there seems to be a nearly empty space instead of a region with deposited particles as without ultrasonic agitation. This can be seen more clearly in figure 4.7, another SEM image that shows a bigger part of the edge of the ring.

Since ultrasonic agitation leads to shock waves within the drying droplet, it is possible that these waves facilitate mass transport in the solution as it evaporates. Since these shock waves propagate in random directions throughout the droplet, such a mass transport is very turbulent and will thus weaken the effect of the flow to the edge of the drying droplet. This means that clusters of spheres and chains of GNRs will be deposited more evenly over the surface of the substrate and not only at the edges of the droplet, which would explain the lower concentration of deposited particles near the edge of the droplet with ultrasonic agitation.

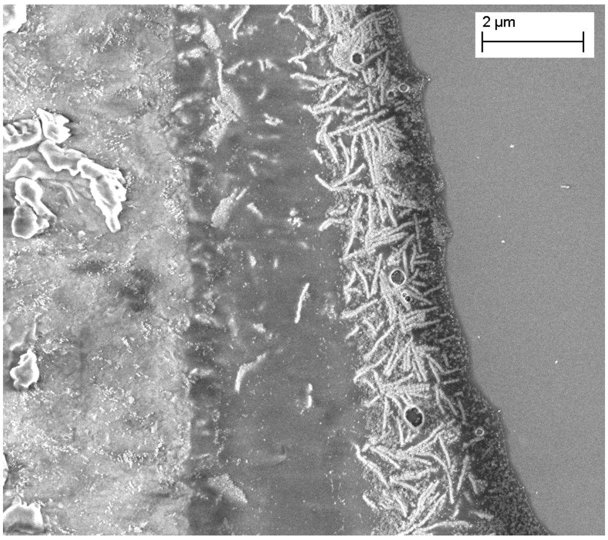

Figure 4.7: A SEM image of the substrate with solution RS that was ultrasonically agitated showing a nearly empty space at about 2 µm from the edge of the ring.

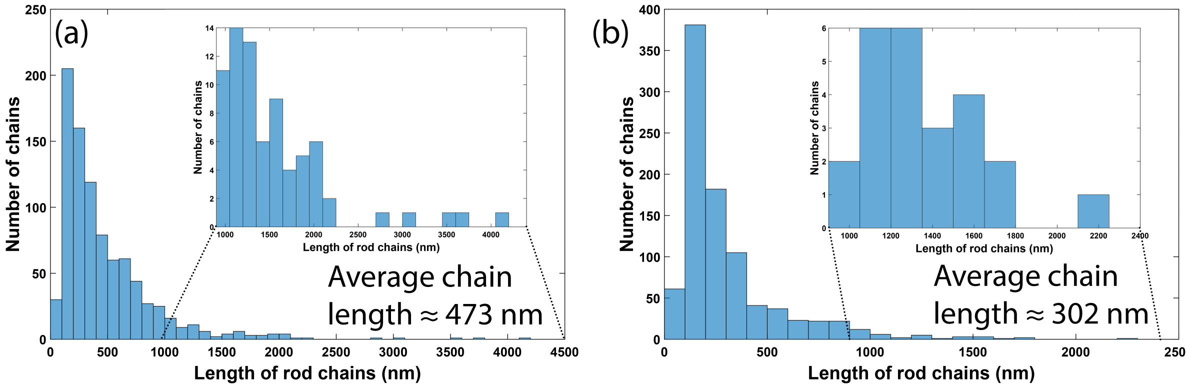

Figure 4.8: Histograms showing the lengths of the chains that were measured. (a) shows collected data for the substrate that was not agitated ultrasonically, (b) shows the collected data for the substrate that was agitated ultrasonically. The insets show a larger image of the data in the histograms for chain lengths of 1000 nm and higher.

As mentioned earlier, GNRs are expected to form plate-shaped clusters due the preferred side-by-side assembly while spheres form spherical superstructures. As was also mentioned earlier, shock waves in the droplet are expected to cause more and stronger collisions, breaking up the assembled superstructures. Since superstructures of GNRs are expected to break more easily than superstructures of spheres (think of the difference between breaking a pen in half and breaking a ball in half), this means that structures of GNRs will generally be smaller than structures of spheres. This causes them to be more easily influenced by the effect of the flow to the edge of the droplet, which is why this is expected to be the reason that there are so many more GNRs found at the edge of the droplet.

Why this lower concentration of particles at the edge of the ring was not observed in the SEM images of solution R is peculiar but since the only difference between the solutions is the addition of spheres, it must be due to them. Since it's expected that spheres cluster together forming superstructures with relatively large masses, it could be possible that these superstructures deposit somewhere away from the edge of the ring before the droplet has evaporated completely, no longer influenced by the flow within the droplet due to it's large mass. This superstructure can be then disrupt the flow within the droplet, causing less particles to reach the edge of the ring. Since it's expected superstructures of GNRs break more easily than superstructures of gold nanospheres, this is not applicable for solution R.

Unlike the reasons mentioned in the discussion of the observations of solution R on SiO_2 substrates, heating and other differences between the two experiments are not expected to have a noticeable effect on the deposition of solution RS. The increased phase-separation due to ultrasonic agitation is so extreme that it dominates thermal agitation due to heating which is not likely to have caused the differences observed in figure 4.6.

4.4 Deposition on HOPG

Only solution R was deposited on HOPG since the alignment of GNRs at step edges is what is being researched. These substrates were investigated with SEM and AFM.

4.4.1 SEM images

No ultrasonic agitation

Since the surface of HOPG is hydrophobic, the evaporation process is different as compared to the hydrophilic SiO_2 substrates which was explained in chapter 2. Since the contact line slips over the surface, it leaves behind areas with high and low concentrations of GNRs which can be clearly seen in figure 4.9a where the direction of movement is along the diagonal starting from bottom-left to top-right.

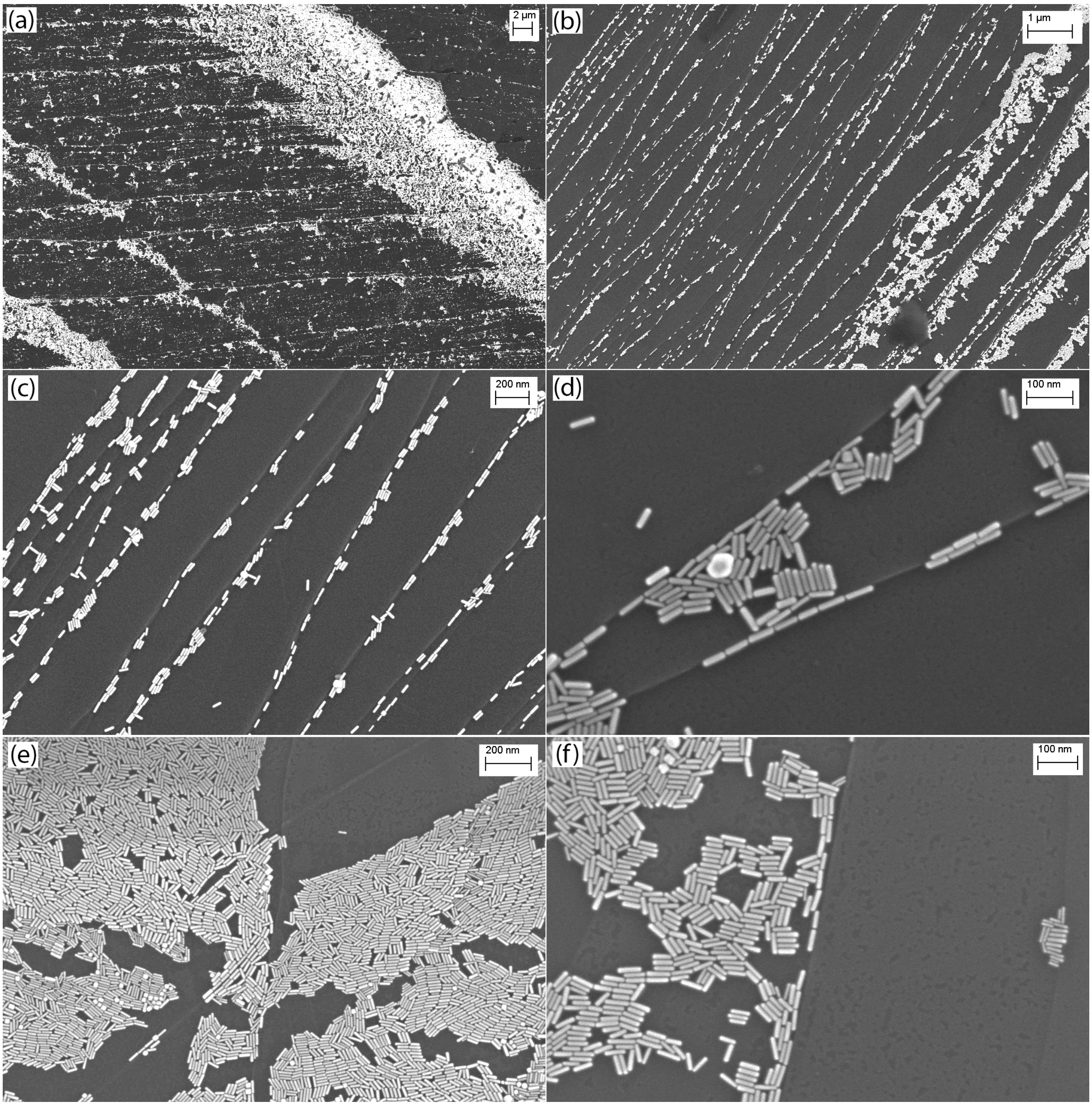

Figure 4.9: Typical SEM images of an evaporated droplet of solution R on an HOPG substrate. (a) is an overview that shows the stick-and-slip motion of the droplet as it evaporates. (b)-(d) show the alignment of GNRs along the step edges of the HOPG. (e) and (f) show GNRs laying on terraces where no definite alignment is seen.

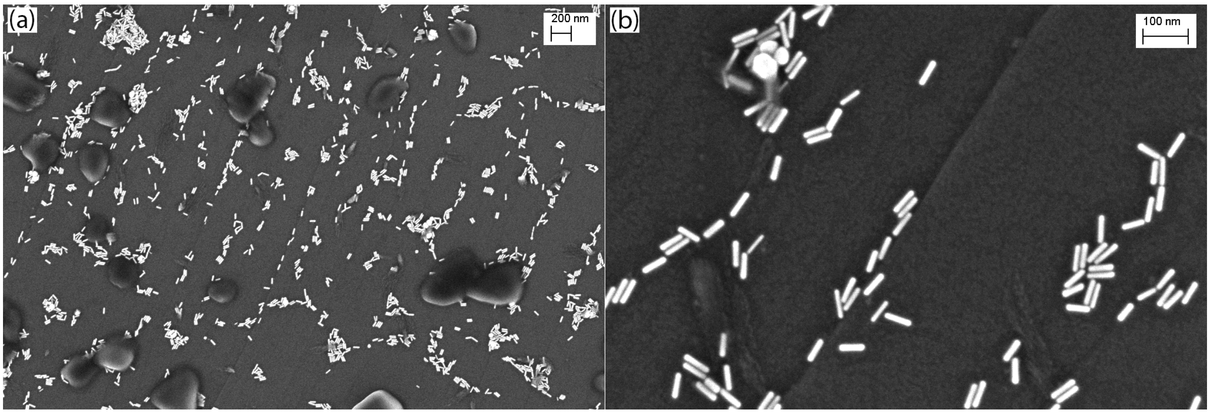

Figure 4.10: Typical SEM images of an evaporated droplet of solution R on an HOPG substrate that was subjected to ultrasonic agitation. (a) shows an overview with step edges and terraces while (b) shows more details.

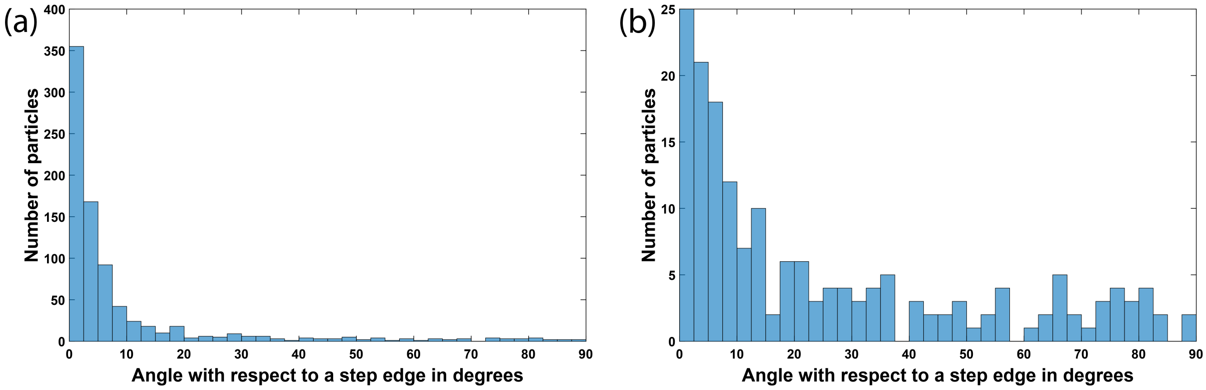

Figure 4.11: Histograms showing the angle of the GNRs with respect to step edges. (a) shows collected data for the substrate that was not agitated ultrasonically, (b) shows the collected data for the substrate that was agitated ultrasonically.

Zooming in a little bit further, it can be seen that most GNRs are neatly aligned parallel to the step edges of the HOPG and in some cases with clusters attached to them, shown in figure 4.9b, 4.9c and 4.9d. When GNRs or clusters of GNRs are laying on terraces, they do not seem to have any certain alignment, as can be seen in figure 4.9e and 4.9f. Something that does stand out, is the fact that GNRs do prefer a side-by-side alignment creating very short chains of GNRs.

Ultrasonic agitation

Figure 4.10 shows SEM images that were obtained when analyzing the substrate that was subjected to ultrasonic agitation. A couple of things are observed when comparing these images to the ones in figure 4.9. Even though the step edges are a bit difficult to see in some of the images, it is possible to make them out by looking at the orientation of the GNRs. Again the GNRs do seem to align parallel to the step edges, but they seem to be clustered together less often and more (small) clusters and/or loose GNRs are observed on the terraces away from the step edges. More than without agitation, GNRs seem to be everywhere on the substrate instead of being concentrated near the step edges. For this thesis, a good way to analyze these images quantitatively was not found in order to determine whether or not this observation is accurate due to the unclear step edges in the images.

Next, it seems that when GNRs are aligned to the step edges, more GNRs are aligned parallel to the edges in the case of no ultrasonic agitation than in the case of ultrasonic agitation. The orientation of the GNRs at the step edges was measured quantitatively for both cases using a method that first defines the step edge and then measures the angle of a rod with respect to this edge. Only GNRs that

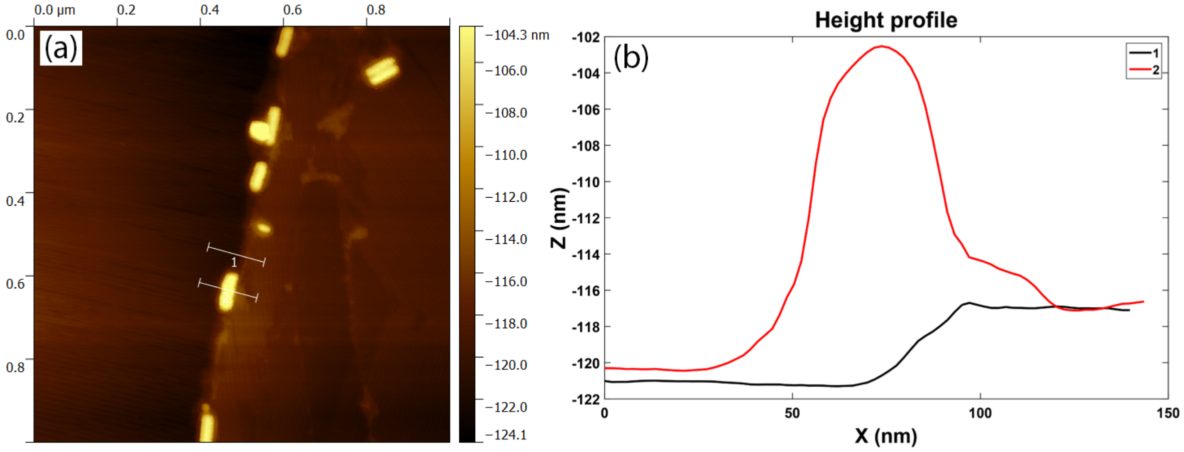

Figure 4.12: (a) an AFM image of GNRs on HOPG showing that GNRs align along the step edge. (b) the height profile taken at the step edge showing that GNRs lie on the lower step of the step edge.

were ‘touching’ the step edges were taken into account. The results can be seen in figure 4.11a and b, which show histograms of the collected data. Figure 4.11a shows the data of the substrate that was not ultrasonically agitated, while b shows the data of the substrate that was ultrasonically agitated. When comparing the two, a clear difference can be seen since in (a) the largest peak is seen near an angle of 0^o, meaning the GNRs are aligned parallel to the step edge. Even though the largest bar in (b) is also near 0^o, the bars for other angles are relatively much higher. GNRs seem to be oriented much more randomly in (b) than in (a), confirming that more GNRs are aligned parallel to the step edge in the case of no ultrasonic agitation.

The measurements indicate that the GNRs prefer to deposit at the step edges on the HOPG substrate, which we expect is caused by van der Waals forces. The HOPG surface is relatively closer to a GNR laying at the bottom of and parallel to a step edge, which causes an increased van der Waals interaction between the GNR and the surface. So when a GNR comes near a step edge just before assembling, the van der Waals forces will ‘trap’ it at the bottom side of the edge. The van der Waals forces also explain the preferred alignment of GNRs with the step edge, since the HOPG surface is relatively closest to the GNR when its longitudinal axis is aligned with the step edge.

For the images of the substrates with ultrasonic agitation it is observed that less GNRs seem to be aligned to (or even near) the step edges, which suggest that something pushed the GNRs away from the edges. We expect that the reason for this could be one of two things; the shock waves from the ultrasonic agitation or the accidental rise in temperature during the process. The shock waves cause stronger currents, which seem to dominate the van der Waals forces and push the GNRs away from the step edges. The temperature rise increases the Brownian motion giving the particles more energy, which could also be enough to dominate the van der Waals forces. Which of these to possibilities dominates the effect cannot be determined, an experiment in which both substrates were kept at the same temperature should be able to answer this.

4.4.2 AFM images

The HOPG substrates were placed under an AFM in order to investigate on which terrace the GNRs were laying when aligned parallel to the step edge. Figure 4.12a shows an AFM image of GNRs at a step edge. Figure 4.12b shows the height profile of the image in (a), where two things can be observed. By looking at height profile 1, it can be concluded that the left terrace is lower than the right terrace. Furthermore, by looking at height profile 2 it can be concluded that the GNRs are laying on the bottom terrace as well as that the GNRs have a greater height (or diameter) than the step edge itself.

Something else that was found during the investigation of the HOPG substrates with AFM that is beyond the scope of this assignment is shown in figure 4.13. What can be observed on the terraces of the HOPG are regularly spaced and oriented stripes. They cannot be an artifact of the machine since they are not

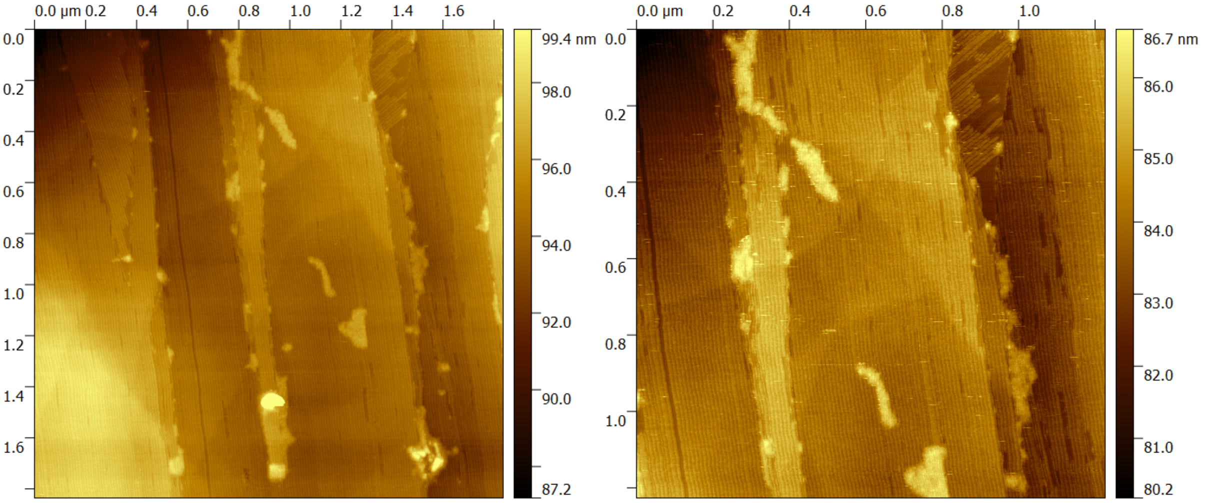

Figure 4.13: AFM images showing the stripes on the terraces of the HOPG. In the image on the left stripes with different orientations can be seen, while the figure on the right is zoomed some a bit and show the stripes more clearly.

observed in every AFM image, they are observed in different orientations and they sometimes have defects. It is suspected that these stripes are molecules of CTAB that are neatly packed together in a manner that is energetically most favorable. Unfortunately, it is very hard to get a correct measurement for the height profile of the observed stripes since they are very close together. So close in fact, that it could be possible that the AFM tip is too big to fully reach down between the molecules while working, meaning that it does not give an accurate height measurement.

In order to test this theory, a height profile was taken in a large defect; large enough that the AFM tip was able to measure the height correctly. This measurement is shown in figure 4.14. It can be seen that the height difference stays about constant in the defect, meaning that 1 nm is the actual height of a stripe. The height profile taken of the stripes without defects only shows a height difference of about 0,1 nm, meaning the AFM tip is indeed to large to measure the height correctly. These height differences of 1 nm and 0,1 nm were also seen in other images where defects were analyzed. Since the length of a fully stretched CTA$^+$ ion is about 2,2 nm [65] and the diameter of a CTAB micelle is about 4,4 nm [66], arguments involving these factors cannot be used directly to explain the 1 nm height difference. In order to find the correct explanation, more research is needed.

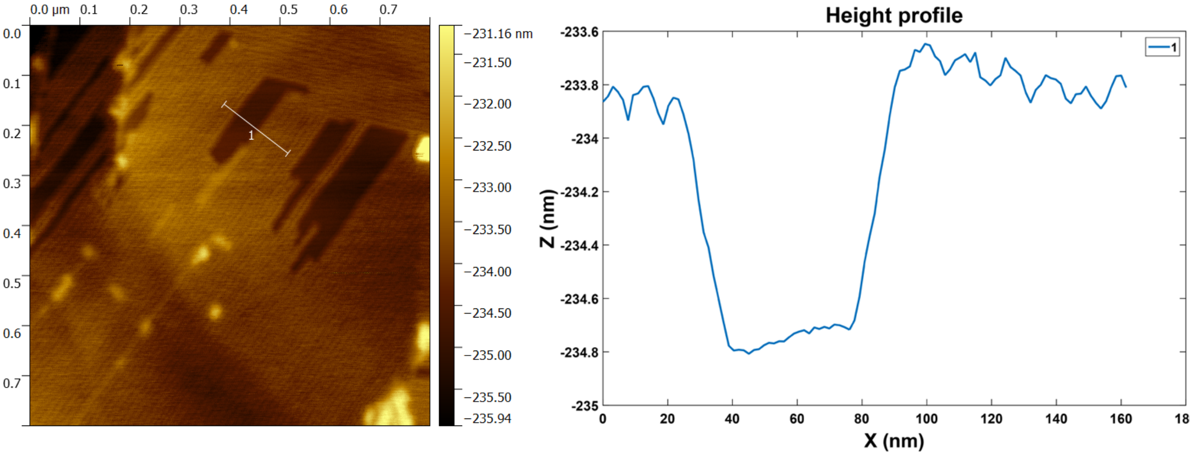

Figure 4.14: The image on the left is an AFM image showing stripes on the terraces of the HOPG, with some defects in them. The figure on the right shows the height profile that is obtained when measuring the image from left to right. It can be seen that the depth of the defect stays almost constant at about 1 nm.

5 Conclusions and recommendations

The effect of ultrasonic vibration on the deposition of GNRs and gold nanospheres on a SiO_2 substrate and the deposition of GNRs on a HOPG substrate have been analyzed. This effect has been measured by making SEM and AFM images of the depositions.

Two droplets of solution R (a solution with mostly rods) and solution RS (a solution with both rods and spheres) were placed on SiO_2 substrates and were left to dry. One of each pair of the droplets was ultrasonically agitated during the evaporation process, while the other was left undisturbed. When the droplets evaporated completely, the result was a coffee-stain ring. For the deposition of solution R a higher ordering of GNRs was observed when the droplet was ultrasonically agitated. There is however a big chance that this effect is not due to the ultrasonic agitation, but due to a rise in temperature of the ultrasonic bath during the evaporation of the droplet. Ultrasonic agitation does seem to have a noticeable effect on the deposition of solution RS. The SEM images of the deposition without ultrasonic agitation agree with the existing theory, while for the deposition with ultrasonic agitation a very different assembly was observed than without the agitation. In this case only GNRs were observed at the edge of the coffee-stain ring and the gold nanospheres were deposited elsewhere in the droplet, away from the three-phase contact line. Furthermore, the maximum and average chain lengths of the GNRs of the deposition with ultrasonic agitation were shorter than without ultrasonic agitation. It is expected that the shock waves caused by the agitation cause these effects by increasing the number and the power of collisions between superstructures. This breaks the superstructures into smaller superstructures, resulting in the deposition of smaller chains of GNRs.

Two droplets of solution R were deposited on HOPG substrates. One of the substrates was ultrasonically agitated, while the other was left undisturbed. Because HOPG is hydrophobic, in contrary to the hydrophilic SiO_2, the droplet had no fixed contact line during the evaporation process. The contact line followed a stick-slip motion, leaving behind rings of GNRs. For the deposition without ultrasonic agitation, the GNRs were deposited at the bottom of and parallel to the step edges of the HOPG. It's expected that this behaviour originates from a more favourable position due to a stronger van der Waals interaction with the surface. For the deposition with ultrasonic agitation, alignment of the rods parallel to the step edges was observed less often. It is not certain if this is due to the ultrasonic agitation or due to the temperature rise of the ultrasonic bath during the experiment.

For further research we suggest to repeat the deposition measurements both with and without ultrasonic agitation, while keeping environmental factors, like temperature and humidity, more equal. Especially a measurement with and without ultrasonic agitation where the temperature is equal for both measurements is interesting, since it is expected that some of the observations were caused by a rise in temperature of the ultrasonic bath. While making the SEM images of these new depositions on HOPG, one should make sure that the step edges are clearly seen in the images. In many of the images made during this thesis the step edges were hardly visible, making it impossible to measure the difference in concentration of GNRs on the terraces versus GNRs aligned along the step edges. Furthermore we suggest to change the frequency of the ultrasonic bath to see what the effect is on the assembly and orientation of GNRs and gold nanospheres on both SiO_2 and HOPG substrates. Lastly we recommend to further research the encountered (CTAB) stripes on the HOPG samples since this is still an unknown phenomenon.

6 References

[1] M. A. El-Sayed, “Some interesting properties of metals confined in time and nanometer space of different shapes,” *Accounts of chemical research*, vol. 34, no. 4, pp. 257–264, 2001.

[2] M.-C. Daniel and D. Astruc, “Gold nanoparticles: assembly, supramolecular chemistry, quantum-size-related properties, and applications toward biology, catalysis, and nanotechnology,” *Chemical reviews*, vol. 104, no. 1, pp. 293–346, 2004.

[3] C. Burda, X. Chen, R. Narayanan, and M. A. El-Sayed, “Chemistry and properties of nanocrystals of different shapes,” *Chemical reviews*, vol. 105, no. 4, pp. 1025–1102, 2005.

[4] M. A. El-Sayed, “Small is different: shape-, size-, and composition-dependent properties of some colloidal semiconductor nanocrystals,” *Accounts of chemical research*, vol. 37, no. 5, pp. 326–333, 2004.

[5] A. P. Alivisatos, “Perspectives on the physical chemistry of semiconductor nanocrystals,” *The Journal of Physical Chemistry*, vol. 100, no. 31, pp. 13226–13239, 1996.

[6] S. Nie and S. R. Emory, “Probing single molecules and single nanoparticles by surface-enhanced raman scattering,” *science*, vol. 275, no. 5303, pp. 1102–1106, 1997.

[7] G. Schmid, “Large clusters and colloids. metals in the embryonic state,” *Chemical Reviews*, vol. 92, no. 8, pp. 1709–1727, 1992.

[8] C. J. Murphy, L. B. Thompson, D. J. Chernak, J. A. Yang, S. T. Sivapalan, S. P. Boulos, J. Huang, A. M. Alkilany, and P. N. Sisco, “Gold nanorod crystal growth: from seed-mediated synthesis to nanoscale sculpting,” *Current Opinion in Colloid & Interface Science*, vol. 16, no. 2, pp. 128–134, 2011.

[9] C. J. Murphy, T. K. Sau, A. M. Gole, C. J. Orendorff, J. Gao, L. Gou, S. E. Hunyadi, and T. Li, “Anisotropic metal nanoparticles: synthesis, assembly, and optical applications,” *The Journal of Physical Chemistry B*, vol. 109, no. 29, pp. 13857–13870, 2005.

[10] A. J. Haes, D. A. Stuart, S. Nie, and R. P. Van Duyne, “Using solution-phase nanoparticles, surface-confined nanoparticle arrays and single nanoparticles as biological sensing platforms,” *Journal of fluorescence*, vol. 14, no. 4, pp. 355–367, 2004.

[11] A. K. Salem, P. C. Searson, and K. W. Leong, “Multifunctional nanorods for gene delivery,” *Nature materials*, vol. 2, no. 10, pp. 668–671, 2003.

[12] Y.-Y. Yu, S.-S. Chang, C.-L. Lee, and C. C. Wang, “Gold nanorods: electrochemical synthesis and optical properties,” *The Journal of Physical Chemistry B*, vol. 101, no. 34, pp. 6661–6664, 1997.

[13] B. Nikoobakht and M. A. El-Sayed, “Surface-enhanced raman scattering studies on aggregated gold nanorods,” *The Journal of Physical Chemistry A*, vol. 107, no. 18, pp. 3372–3378, 2003.

[14] B. Nikoobakht, J. Wang, and M. A. El-Sayed, “Surface-enhanced raman scattering of molecules adsorbed on gold nanorods: off-surface plasmon resonance condition,” *Chemical Physics Letters*, vol. 366, no. 1, pp. 17–23, 2002.

[15] J. Pérez-Juste, I. Pastoriza-Santos, L. M. Liz-Marzán, and P. Mulvaney, “Gold nanorods: synthesis, characterization and applications,” *Coordination Chemistry Reviews*, vol. 249, no. 17, pp. 1870–1901, 2005.

[16] A. Alekseeva, V. Bogatyrev, B. Khlebtsov, A. Mel'nikov, L. Dykman, and N. Khlebtsov, "Gold nanorods: synthesis and optical properties," *Colloid Journal*, vol. 68, no. 6, pp. 661–678, 2006.

[17] V. Sharma, K. Park, and M. Srinivasarao, "Colloidal dispersion of gold nanorods: Historical background, optical properties, seed-mediated synthesis, shape separation and self-assembly," *Materials Science and Engineering: R: Reports*, vol. 65, no. 1, pp. 1–38, 2009.

[18] B. Nikoobakht and M. A. El-Sayed, "Preparation and growth mechanism of gold nanorods (nrs) using seed-mediated growth method," *Chemistry of Materials*, vol. 15, no. 10, pp. 1957–1962, 2003.

[19] M. Grzelczak, J. Pérez-Juste, P. Mulvaney, and L. M. Liz-Marzán, "Shape control in gold nanoparticle synthesis," *Chemical Society Reviews*, vol. 37, no. 9, pp. 1783–1791, 2008.

[20] X. Jiang and M. Pileni, "Gold nanorods: influence of various parameters as seeds, solvent, surfactant on shape control," *Colloids and Surfaces A: Physicochemical and Engineering Aspects*, vol. 295, no. 1, pp. 228–232, 2007.

[21] B. Dan, T. B. Wingfield, J. S. Evans, F. Mirri, C. L. Pint, M. Pasquali, and I. I. Smalyukh, "Templating of self-alignment patterns of anisotropic gold nanoparticles on ordered swnt macrostructures," *ACS applied materials & interfaces*, vol. 3, no. 9, pp. 3718–3724, 2011.

[22] G. A. Ozin, K. Hou, B. V. Lotsch, L. Cademartiri, D. P. Puzzo, F. Scotognella, A. Ghadimi, and J. Thomson, "Nanofabrication by self-assembly," *Materials Today*, vol. 12, no. 5, pp. 12–23, 2009.

[23] I. Ahmad, H. J. Zandvliet, and E. S. Kooij, "Shape-induced separation of nanospheres and aligned nanorods," *Langmuir*, vol. 30, no. 27, pp. 7953–7961, 2014.

[24] K. J. Bishop, C. E. Wilmer, S. Soh, and B. A. Grzybowski, "Nanoscale forces and their uses in self-assembly," *small*, vol. 5, no. 14, pp. 1600–1630, 2009.

[25] M. H. Lash, M. V. Fedorchak, S. R. Little, and J. J. McCarthy, "Fabrication and characterization of non-brownian particle-based crystals," *Langmuir*, 2014.

[26] N. R. Jana, L. Gearheart, and C. J. Murphy, "Wet chemical synthesis of high aspect ratio cylindrical gold nanorods," *The Journal of Physical Chemistry B*, vol. 105, no. 19, pp. 4065–4067, 2001.

[27] J. Zhang, N. Balla, C. Gao, C. J. Sheppard, L. Yung, S. Rehman, J. Teo, S. Kulkarni, Y. Fu, and S. J. Yin, "Surface modified gold nanorods in two photon luminescence imaging," *Australian Journal of Chemistry*, vol. 65, no. 3, pp. 290–298, 2012.

[28] A. Gole and C. J. Murphy, "Seed-mediated synthesis of gold nanorods: role of the size and nature of the seed," *Chemistry of Materials*, vol. 16, no. 19, pp. 3633–3640, 2004.

[29] N. R. Jana, L. Gearheart, and C. J. Murphy, "Wet chemical synthesis of high aspect ratio cylindrical gold nanorods," *The Journal of Physical Chemistry B*, vol. 105, no. 19, pp. 4065–4067, 2001.

[30] T. K. Sau and C. J. Murphy, "Seeded high yield synthesis of short au nanorods in aqueous solution," *Langmuir*, vol. 20, no. 15, pp. 6414–6420, 2004.

[31] J. Cheng, L. Ge, B. Xiong, and Y. He, "Investigation of ph effect on gold nanorod synthesis," *Journal of the Chinese Chemical Society*, vol. 58, no. 6, pp. 822–827, 2011.

[32] J. Gao, C. M. Bender, and C. J. Murphy, "Dependence of the gold nanorod aspect ratio on the nature of the directing surfactant in aqueous solution," *Langmuir*, vol. 19, no. 21, pp. 9065–9070, 2003.

[33] M. Liu and P. Guyot-Sionnest, "Mechanism of silver (i)-assisted growth of gold nanorods and bipyramids," *The Journal of Physical Chemistry B*, vol. 109, no. 47, pp. 22192–22200, 2005.

[34] F. Hubert, F. Testard, and O. Spalla, "Cetyltrimethylammonium bromide silver bromide complex as the capping agent of gold nanorods," *Langmuir*, vol. 24, no. 17, pp. 9219–9222, 2008.

[35] K. A. Willets and R. P. Van Duyne, "Localized surface plasmon resonance spectroscopy and sensing," *Annu. Rev. Phys. Chem.*, vol. 58, pp. 267–297, 2007.

[36] E. S. Kooij and B. Poelsema, "Shape and size effects in the optical properties of metallic nanorods," *Physical Chemistry Chemical Physics*, vol. 8, no. 28, pp. 3349–3357, 2006.

[37] G. Mie, “Beiträge zur optik trüber medien, speziell kolloidaler metallösungen,” *Annalen der physik*, vol. 330, no. 3, pp. 377–445, 1908.

[38] C. Kumar, *UV-VIS and Photoluminescence Spectroscopy for Nanomaterials Characterization*. Springer, 2013.

[39] F. Young, *Cavitation*. McGraw-Hill, 1989.

[40] T. Leong, M. Ashokkumar, and S. Kentish, “The fundamentals of power ultrasound–a review,” *Acoustics Australia*, vol. 39, no. 2, pp. 54–63, 2011.

[41] K. S. Suslick, J. W. Goodale, P. F. Schubert, and H. H. Wang, “Sonochemistry and sonocatalysis of metal carbonyls,” *Journal of the American Chemical Society*, vol. 105, no. 18, pp. 5781–5785, 1983.

[42] T. Leong, T. Wooster, S. Kentish, and M. Ashokkumar, “Minimising oil droplet size using ultrasonic emulsification,” *Ultrasonics Sonochemistry*, vol. 16, no. 6, pp. 721–727, 2009.

[43] R. Singla, M. Ashokkumar, and F. Grieser, “The mechanism of the sonochemical degradation of benzoic acid in aqueous solutions,” *Research on chemical intermediates*, vol. 30, no. 7-8, pp. 723–733, 2004.

[44] M. Mastrangeli, S. Abbasi, C. Varel, C. Van Hoof, J.-P. Celis, and K. F. Böhringer, “Self-assembly from milli-to nanoscales: methods and applications,” *Journal of micromechanics and microengineering*, vol. 19, no. 8, p. 083001, 2009.

[45] Y. Li, T. Kunitake, and S. Fujikawa, “Efficient fabrication of large, robust films of 3d-ordered polystyrene latex,” *Colloids and Surfaces A: Physicochemical and Engineering Aspects*, vol. 275, no. 1, pp. 209–217, 2006.

[46] B. A. Korgel and D. Fitzmaurice, “Self-assembly of silver nanocrystals into two-dimensional nanowire arrays,” *Advanced Materials*, vol. 10, no. 9, pp. 661–665, 1998.

[47] B. Nikoobakht, Z. Wang, and M. El-Sayed, “Self-assembly of gold nanorods,” *The Journal of Physical Chemistry B*, vol. 104, no. 36, pp. 8635–8640, 2000.

[48] M.-P. Pileni, “Nanocrystal self-assemblies: fabrication and collective properties,” *The Journal of Physical Chemistry B*, vol. 105, no. 17, pp. 3358–3371, 2001.

[49] C. Collier, T. Vossmeyer, and J. Heath, “Nanocrystal superlattices,” *Annual Review of Physical Chemistry*, vol. 49, no. 1, pp. 371–404, 1998.

[50] S. Ahmed and K. M. Ryan, “Self-assembly of vertically aligned nanorod supercrystals using highly oriented pyrolytic graphite,” *Nano letters*, vol. 7, no. 8, pp. 2480–2485, 2007.

[51] D. A. Walker, B. Kowalczyk, M. O. de La Cruz, and B. A. Grzybowski, “Electrostatics at the nanoscale,” *Nanoscale*, vol. 3, no. 4, pp. 1316–1344, 2011.

[52] K. J. Bishop, C. E. Wilmer, S. Soh, and B. A. Grzybowski, “Nanoscale forces and their uses in self-assembly,” *small*, vol. 5, no. 14, pp. 1600–1630, 2009.

[53] D. Mampallil, “Some physics inside drying droplets,” *Resonance*, vol. 19, no. 2, pp. 123–134, 2014.

[54] H. Hu and R. G. Larson, “Analysis of the microfluid flow in an evaporating sessile droplet,” *Langmuir*, vol. 21, no. 9, pp. 3963–3971, 2005.

[55] H. Bodiguel and J. Leng, “Imaging the drying of a colloidal suspension,” *Soft Matter*, vol. 6, no. 21, pp. 5451–5460, 2010.

[56] H. B. Eral, D. M. Augustine, M. H. Duits, and F. Mugele, “Suppressing the coffee stain effect: how to control colloidal self-assembly in evaporating drops using electrowetting,” *Soft Matter*, vol. 7, no. 10, pp. 4954–4958, 2011.

[57] Á. G. Marín, H. Gelderblom, D. Lohse, and J. H. Snoeijer, “Order-to-disorder transition in ring-shaped colloidal stains,” *Physical review letters*, vol. 107, no. 8, p. 085502, 2011.

[58] R. D. Deegan, O. Bakajin, T. F. Dupont, G. Huber, S. R. Nagel, and T. A. Witten, “Capillary flow as the cause of ring stains from dried liquid drops,” *Nature*, vol. 389, no. 6653, pp. 827–829, 1997.

[59] N. Yasarawan and J. S. van Duijneveldt, “Arrested phase separation of colloidal rod–sphere mixtures,” *Soft Matter*, vol. 6, no. 2, pp. 353–362, 2010.

[60] M. Adams, Z. Dogic, S. L. Keller, and S. Fraden, “Entropically driven microphase transitions in mixtures of colloidal rods and spheres,” *Nature*, vol. 393, no. 6683, pp. 349–352, 1998.

[61] T. K. Sau and C. J. Murphy, “Self-assembly patterns formed upon solvent evaporation of aqueous cetyltrimethylammonium bromide-coated gold nanoparticles of various shapes,” *Langmuir*, vol. 21, no. 7, pp. 2923–2929, 2005.

[62] A. Kuijk, D. V. Byelov, A. V. Petukhov, A. van Blaaderen, and A. Imhof, “Phase behavior of colloidal silica rods,” *Faraday discussions*, vol. 159, no. 1, pp. 181–199, 2012.

[63] I. Kholmanov, E. Cavaliere, M. Fanetti, C. Cepek, and L. Gavioli, “Growth of curved graphene sheets on graphite by chemical vapor deposition,” *Physical Review B*, vol. 79, no. 23, p. 233403, 2009.

[64] M. Shimonaka, Y. Nakamura, J. Kikkawa, and A. Sakai, “Self-assembly of ge clusters on highly oriented pyrolytic graphite surfaces,” *Surface Science*, vol. 628, pp. 82–85, 2014.

[65] T. K. Sau and C. J. Murphy, “Self-assembly patterns formed upon solvent evaporation of aqueous cetyltrimethylammonium bromide-coated gold nanoparticles of various shapes,” *Langmuir*, vol. 21, no. 7, pp. 2923–2929, 2005.

[66] V. Aswal, P. Goyal, and P. Thiyagarajan, “Small-angle neutron-scattering and viscosity studies of ctab/nasal viscoelastic micellar solutions,” *The Journal of Physical Chemistry B*, vol. 102, no. 14, pp. 2469–2473, 1998.

[67] W. Haiss, N. T. Thanh, J. Aveyard, and D. G. Fernig, “Determination of size and concentration of gold nanoparticles from uv-vis spectra,” *Analytical chemistry*, vol. 79, no. 11, pp. 4215–4221, 2007.

Appendix A

Calculating the concentration of particles in a solution

The concentration of spherical particles in a solution can be calculated by using formula A.1 [67], where N is the number density of particles per unit volume, A is the absorption that was measured using UV-VIS, b is the diameter of the spheres, Q_{ext} is the extinction efficiency and d_0 is the path length of the spectrometer that was used.

In order to calculate the density of rods in both solutions, formula A.1 was adapted for rod shape particles, taking into account their aspect ratio and short radius, where η is the aspect ratio of the rods and a is the short radius of the rods.

Table A.1 shows the concentrations that were obtained for solution R and solution RS. This leads to a ratio of spheres to rods of about 8,7 to 1.

$$N = \frac{A \cdot 2,303}{\pi \cdot b^2 \cdot Q_{ext} \cdot d_0} \tag{A.1}$$

$$N = \frac{A \cdot 2,303}{\pi \cdot \eta^{\frac{2}{3}} \cdot a^2 \cdot Q_{ext} \cdot d_0} \tag{A.2}$$

	Concentration of rods (per cm^3)	Concentration of spheres (per cm^3)
Solution R	5,34 × 10^{10}	-
Solution RS	1,40 × 10^{10}	1,22 × 10^{11}

Table A.1: The calculated concentrations of rods and spheres in solution R and solution RS.

Appendix B

Simulating absorption spectra

By simulating the absorption spectra for solutions containing GNRs with different distributions of ARs using the quasi-static approximation, the effect of the distribution of the AR on the longitudinal peak position in the absorption spectra was studied. As a reference, the absorption spectra of solutions containing GNRs of only one AR were simulated for ARs 2-7 (figure B.1a). By comparing this figure to figure 2.5, it can be seen that these simulations agree with the earlier work of the PIN group.

At the end of section 2.2 it is stated that, for solutions containing GNRs with the same mean AR, the longitudinal peak position in the absorption spectrum of a solution containing GNRs with a normal distribution for the AR (λ_{norm}) is located at a higher wavelength than the longitudinal peak position of a solution containing GNRs of one AR (λ_0). Figure B.1b shows simulated absorption spectra of solutions containing GNRs of which the ARs follow a normal distribution with a standard deviation (σ) equal to 30% of the mean AR. Comparing this figure to figure B.1a indeed shows that λ_{norm} is located at a higher wavelength than λ_0 and that the difference between the two peak positions seems to increase with increasing mean AR of the GNRs. To confirm this the difference is plotted against the AR for normal distributions of the AR with a σ of 10%, 20% and 30% of the mean AR (figure B.1c). Figure B.1c shows that the difference between λ_{norm} and λ_0 increases for increasing width of the distribution of the AR. The deviation from λ_0 becomes significant indicating that the distribution of the AR is an important parameter when estimating the AR of a solution.

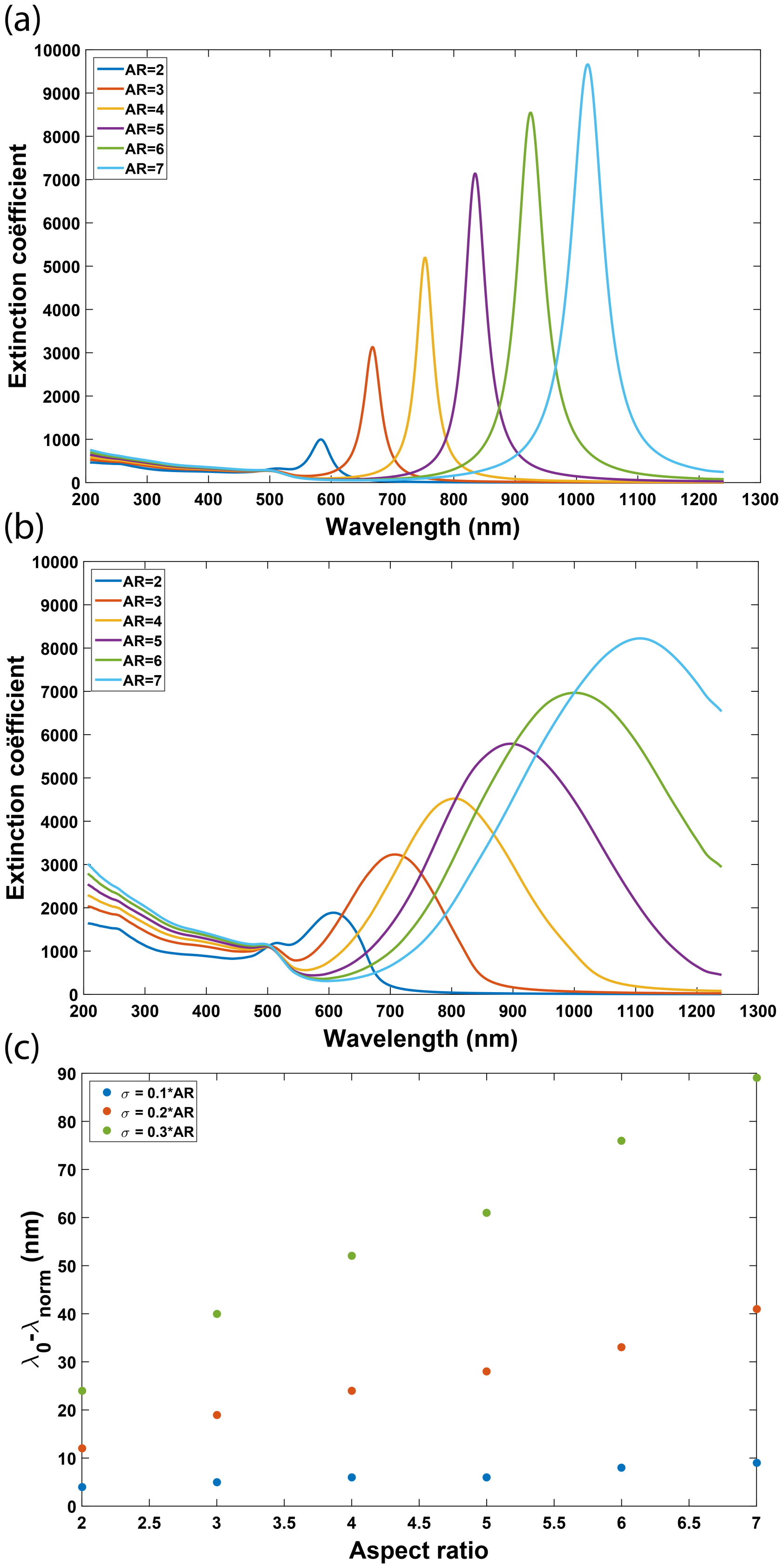

Figure B.1: The simulated absorption spectra of solutions containing GNRs with a mean AR of 2-7 are plotted for solutions (a) containing GNRs of one AR and (b) containing GNRs with a normal distribution for the AR (σ = 30% of the mean AR). (c) The difference between λ_0 and λ_{norm} is plotted against the AR for normal distributions of the AR with a σ of 10%, 20% and 30% of the mean AR.